The apicoplast link to fever-survival and artemisinin-resistance in the malaria parasite

Min Zhang[a,1], Chengqi Wang[a,1], Jenna Oberstaller[a,1], Phaedra Thomas[a], Thomas D. Otto[b,c], Debora Casandra[a], Sandhya Boyapalle[a], Swamy R. Adapa[a], Shulin Xu[a], Katrina Button-Simons[d], Matthew Mayho[b], Julian C. Rayner[b,e], Michael T. Ferdig[e], Rays H. Y. Jiang[a], John H. Adams[a,2]

[a]Center for Global Health and Infectious Diseases Research and USF Genomics Program, College of Public Health, University of South Florida, 3720 Spectrum Blvd, Suite 404, Tampa, Florida 33612, USA

[b]Wellcome Sanger Institute, Wellcome Genome Campus, Hinxton Cambridgeshire, CB10 1SA United Kingdom

[c]Institute of Infection, Immunity and Inflammation, MVLS, University of Glasgow, Glasgow G12 8TA United Kingdom

[d]Eck Institute for Global Health, Department of Biological Sciences, University of Notre Dame, Notre Dame, IN 46556

[e]Cambridge Institute for Medical Research, University of Cambridge, Cambridge Biomedical Campus, The Keith Peters Building, Hills Road, Cambridge, Cambridgeshire, CB2 0XY United Kingdom

[1] M.Z., C.W. and J.O. contributed equally to this work.

[2]To whom correspondence should be addressed. Email: ja2@usf.edu

ABSTRACT

Background: The emergence and spread of *Plasmodium falciparum* parasites resistant to front-line antimalarial artemisinin-combination therapies (ACT) threatens to erase the considerable gains against the disease of the last decade. We developed a new large-scale phenotypic screening pipeline and used it to carry out the first large-scale forward-genetic phenotype screen in *P. falciparum* to identify genes that allow parasites to survive febrile temperatures.

Results: Screening identified more than 200 *P. falciparum* mutants with differential responses to increased temperature. These mutants were more likely to be sensitive to artemisinin derivatives as well as to heightened oxidative stress. Major processes critical for *P. falciparum* tolerance to febrile temperatures and artemisinin included highly essential, conserved pathways associated with protein-folding, heat-shock and proteasome-mediated degradation, and unexpectedly, isoprenoid biosynthesis, which originated from the ancestral genome of the parasite's algal endosymbiont-derived plastid, the apicoplast. Apicoplast-targeted genes in general were up-regulated in response to heat shock, as were other *Plasmodium* genes with orthologs in plant and algal genomes.

Conclusions*: Plasmodium falciparum* parasites appear to exploit their innate febrile-response mechanisms to mediate resistance to artemisinin. Both responses depend on endosymbiotic cynobacterium-related ancestral genes in the parasite's genome, suggesting a link to the evolutionary origins of *Plasmodium* parasites in free-living ancestors.

Running title: Plastid metabolism enables malaria parasites to survive fever and artemisinin

Key words: genome-wide phenotypic screens, *piggyBac,* QIseq, heat shock, growth fitness, transposon-mediated mutagenesis, phenotypic functional profiling

INTRODUCTION

Malaria remains a leading infectious disease causing >200 million clinical cases and a half-million deaths every year. *Plasmodium falciparum* is the deadliest malaria parasite by far, with growing parasite resistance to front-line antimalarial artemisinin-combination therapies (ACT) threatening to erase the considerable gains against the disease of the last decade. Alarmingly, data indicate that for the first time since 2010, progress in reducing global burden of malaria cases and fatalities nearly flatlined between 2015 and 2017 [1]. New therapies, ideally informed by an understanding of basic parasite biology, are needed to confront these urgent threats to global malaria control. The study of malaria-parasite biology and gene-function has traditionally been limited, because targeted gene-by-gene approaches are laborious and fraught with difficulty due to an AT-rich (~82%) genome that limits scalability of specific targeted gene-editing methods (such as CRISPR). Despite the considerable knowledge gene-by-gene studies have enabled, and the ~two decades that have passed since the *P. falciparum* genome was completed [2], the limited throughput of targeted gene-editing strategies combined with evolutionary distance of *P. falciparum* from classical model eukaryotes has left >90% of genes untouched experimentally, and ~35% of the parasite's ~5474 genes without meaningful functional annotation (www.plasmodb.org) [3]. High-throughput methods for functionally profiling the malaria-parasite genome can hasten development of effective interventions to control a parasite proven to be an adaptable foe.

Parasite-specific processes essential for parasite survival are naturally attractive as potential drug-targets, given the decreased likelihood of deleterious off-target effects to the host. One such process ripe for interrogation is the parasite's survival-response to the extreme conditions of the host's malarial fever. Repeating fever is a hallmark of all types of malaria and the cyclical patterns serve as key diagnostic features of infections. In malignant tertian malaria caused by *P. falciparum,* the 48-hour cycle corresponds to the parasite's asexual intraerythrocytic-stage life-cycle, wherein parasites invade, develop, asexually replicate and then rupture their host red blood cell (RBC) to begin the destructive blood-stage cycle anew. Host fever is triggered by a Type I shock-like response of the innate immune-system exposure to extracellular parasite debris released when infected RBCs are lysed during parasite egress. Malarial fever concomitantly attenuates and synchronizes development of blood-stage *P. falciparum* infections, as it is lethal to all parasite stages except for early intraerythrocytic ring stages. However, parasite tolerance of febrile temperatures is crucial for its successful propagation in human populations as well as a fundamental aspect of malaria pathogenesis. Previous research suggests parasite-specific factors play a role in modulating this tolerance for febrile temperatures, though the identities of many of these factors or the mechanisms by which they operate remain uncertain [4, 5].

We previously used random *piggyBac*-transposon insertional mutagenesis to uncover genes essential for *P. falciparum* blood-stage survival, generating a saturation-level *P. falciparum* mutant library containing ~38,000 single-disruption mutants [6]. We defined 2680 genes as essential for asexual blood-stage growth, including ~1000 *Plasmodium*-conserved genes of unknown function. Here we demonstrate the potential of this *piggyBac*-mutant (*pB*-mutant) library to systematically assign functional annotation to the *P. falciparum* genome by genome-wide phenotypic screens. In this study, we present the

first large-scale forward-genetic functional screen in *P. falciparum* to identify factors linked to parasite survival of febrile temperatures. Importantly, we functionally annotate hundreds of parasite genes as critical for the parasite's response to heat shock (HS) but dispensable under ideal growth-conditions, ~26% of which were previously unannotated with no known function. Expression-profiling the HS-responses in two different heat shock-sensitive (HS-Sensitive) *pB*-mutant clones vs. the wildtype parent NF54 via RNAseq revealed concordance between (1) genes regulated in the parasite's innate response to HS, (2) the processes dysregulated in these mutants vs. wildtype responses to HS, and (3) those mutants we identified as HS-Sensitive in our pooled screens. Together these analyses identify genes and pathways essential in the HS-response, implicating oxidative stress and protein-damage responses, host-cell remodelling, and unexpectedly, apicoplast isoprenoid biosynthesis. Apicoplast-targeted genes in general were up-regulated in response to HS, as were other *Plasmodium* genes with orthologs in plant and algal genomes. Finally, parallel phenotyping of a mutant library revealed a significant overlap between parasite pathways underlying the response to febrile temperatures and those implicated in the artemisinin mechanism of action (MOA), including oxidative stress, protein-damage responses, and apicoplast-mediated vesicular trafficking [7, 8]. Mutants in known protein-targets of artemisinin tended to be sensitive to HS [9], and expression-data from recent field-isolates directly correlates artemisinin-resistance with HS tolerance in our pooled screen [10]. Further, we found the key K13-associated parasite endocytosis pathway linked to artemisinin resistance [11, 12] is also downregulated in response to HS. Together these data identify an unexpected link between artemisinin MOA, HS-survival, and algal origins of the apicoplast, suggesting the parasite exploits its innate fever-response mechanisms to gain resistance to artemisinin. This study creates a blueprint for developing a large-scale phenotypic screening pipeline of the *P. falciparum pB*-mutant library to enable high-throughput

interrogation of phenotypes of interest to hasten further biological insight that can be weaponized against the parasite.

RESULTS

Pooled screens of an extensively characterized pB-mutant clone-library allow robust identification of heat-shock phenotypes

To interrogate pathways and processes associated with parasite survival at febrile temperatures, we developed a large-scale phenotypic screening pipeline to analyze the phenotypes in pooled *pB*-mutant parasites exposed to HS-induced stress (Fig. S1). We previously demonstrated using individual clonal *pB*-mutant parasite lines that mutant growth-phenotypes can be detected and differentiated in pooled screening utilizing QIseq—"Sensitive" mutants with disruptions in genes/genomic features important for growth have lower QIseq reads, while "Neutral" disruptions in features not vital for growth under the same conditions have higher reads [13]. We therefore reasoned that mutants with mutations in genes underlying the HS-response would grow poorly in response to HS compared to mutants in genes not contributing to HS-survival.

We used a pool of 128 unique, extensively characterized *P. falciparum pB*-mutant clones reflecting disruptions in genes spanning a range of functional categories, as well as many genes without existing functional information, as a "pilot-library" for initial phenotypic screen-development ([13, 14]; Methods, *Generating the pilot-library of* pB-*mutant parasite clones*). An *in vitro* HS-screen of this pilot-library, adapted from a phenotype-screen of many *pB*-mutant-clones comprising the pilot-library [15], defined *pB*-mutant HS-response phenotypes to fever-like temperatures (Fig. 1A-E, Table S1A-C, Methods). We next calculated a measure of fitness for each mutant in response to HS while also taking into account inherent differences in mutant-growth in ideal conditions,

which we termed the Phenotypic-Fitness Score in response to HS (PFS_{HS}; Methods). The PFS_{HS} result was consistent with a previously reported flow cytometry-based assay of 25 individual *piggyBac*-mutant clones in response to heat-shock (Wilcoxon $p < 0.01$, Fig 1F; [15]). We classified 28 mutants of the pilot-library as HS-Sensitive (Fig. 1E-H, indicated in red; Table S1A-C). Fourteen mutants performed poorly in both the Growth- and HS-Screens (Fig. 1E,G, yellow). We classified 28 mutants displaying a slight growth advantage in response to HS (Fig. 1E,G, green) as “HS-Tolerant”. Mutants exhibiting neither sensitivity nor tolerance to HS were classified as HS-Neutral (n = 49).

QIseq-data resulting from the HS- and Growth-screens allowed robust assignment of mutant-phenotypes for both (see Methods). We primarily classified mutants sensitive to heat-shock alone as HS-Sensitive to avoid possible over-interpretation of generally-sick Growth-Sensitive mutants (Fig. 1G-H).

Pooled phenotypic screens scaled up to a 1K *pB*-mutant library enable identification of processes driving the *P. falciparum* heat-shock response

We next scaled our pooled HS-screen to a mutant library of 922 functionally uncharacterized mutants using the methods we established in our pilot-library screens (Table S2A-C). This 1K-library comprised 12 large mixed-population pools of uncloned mutants randomly selected from our saturation library and subjected to phenotypic screens in parallel. Insertion-sites were unknown until the 1K-library HS-Screen and QIseq were completed. Mutants were ranked by fold-change growth in response to HS from HS-Sensitive to HS-Tolerant, as per cut-offs determined from our pilot-library screens. Our analysis distinguished 149 mutants growing well in ideal growth conditions but poorly in response to HS as HS-Sensitive (Fig. 2A), while 91 mutants performed poorly in both the Growth- and HS-screens. Of the remaining mutants, 139 HS-Tolerant

mutants had slightly better growth in HS than ideal growth-conditions, while 543 classified as HS-Neutral were neither sensitive nor tolerant.

This larger scale of screening covering genes annotated to diverse GO-categories, as well as many genes of unknown function, allowed us to assess gene functional-enrichment in HS-Sensitive and Growth-Sensitive phenotypic categories vs all other mutants in the 1K-library. HS-Sensitive mutants were enriched in GO terms associated with HS-response such as protein-folding, response to DNA-damage, DNA-repair, and regulation of vesicle-mediated transport, broadly in agreement with processes identified to underlie the HS-response by more conventional gene expression-based methods [4, 5]. Growth-Sensitive mutants tended to be enriched for more general categories broadly important for survival in all conditions, such as translation- or mRNA-metabolism-related terms (Fig. 2B), as might be expected given the high essentiality of these processes in ideal growth [6, 16].

Increased transcription of the unfolded protein response (UPR), organelle-targeted stress-response pathways and host-cell remodeling characterize the parasite HS-response

We first characterized the wildtype parent-NF54 transcriptome in response to HS to establish a baseline for comparison using an experimental design similar to a prior study assessing transcriptional changes in response to febrile temperatures via microarray [5]. The HS assay-design mimicking parasite exposure to malarial fever was modelled after conditions we established for our pooled-screens (Methods). RNAseq was performed on heat-shocked parasites vs. a non-heat-shocked control. Genes identified as differentially expressed in response to febrile temperatures vs. 37°C were classified into three different categories based on direction of response in the wildtype parasite: (1)

upregulated in response to HS; (2) downregulated in HS, and (3) neutral in HS (Fig. 3A-B, Table S3A-D). The majority of genes expressed above threshold in our analysis were HS-neutral (1541 genes out of 2567, or ~60%) and were enriched for genes involved in general housekeeping functions such as the proteasome core complex (ubiquitin-proteasome system), the ubiquitin-dependent ERAD-pathway, and regulators thereof), RNA metabolism (RNA-binding, mRNA-splicing) and transport functions (e.g. protein import into nucleus, vesicle-mediated transport). We primarily considered genes upregulated in HS as drivers of the HS-response.

Genes upregulated in HS (↑, n = 415) tended to be enriched for processes such as protein-folding, unfolded protein-binding, response to heat, mitochondrial processes, and host-cell remodelling-associated exported proteins localizing to the Maurer's clefts (Fig. 3B, Table S3C-D). Genes downregulated in HS (↓, n = 611) tended to be enriched for pathogenesis-related functions and components of the parasite invasion machinery, such as entry/exit from the host cell and cell-cell adhesion, and organelles including the inner-membrane pellicle complex, micronemes, and rhoptries. These data are in general agreement with previously-reported processes expected to drive the parasite HS-response [4, 5].

We reasoned that genes dysregulated in HS-Sensitive mutants compared to wildtype underlie the HS-response. We chose two individual HS-Sensitive mutant clonal lines satisfying several careful criteria for additional profiling via RNAseq to identify dysregulated genes responsible for this sensitivity: *ΔDHC* and *ΔLRR5* (dynein heavy-chain gene PF3D7_1122900 and leucine-rich repeat protein PF3D7_1432400). Criteria for selection: i) Specificity of phenotype. Both mutants are highly sensitive to heat shock (PFS < 0.1), but under ideal culture conditions grow better than most other mutants in

the pilot library (exhibiting higher fold change than 95.3% and 83.6% mutants, respectively). ii) Clear functional consequences of disruption. Both are presumed loss-of-function mutants with a single disruption in the coding region of a gene determined to be dispensable for asexual blood-stage growth under ideal culture conditions[6] . iii) GO classification. GO classifications of LRR5 and DHC are representative of the broad functional categories we found to be associated with heat response in our earlier small screen[15] and other reports (regulating gene expression and intracellular vesicular transport, respectively), yet interactions between these pathways are undefined. Finally, iv) Clonal phenotype validation. Both mutant lines were validated in a heat shock assay of individual clones[15], but otherwise these genes were not previously implicated in the HS-response of malaria parasites.

The 1298 genes which could be classified into HS-response categories across all three parasites were analyzed for functional-enrichment (Table S3B). The majority of genes were HS-neutral across all three parasites and were enriched for essential housekeeping functions (n = 615; Table S3B-D). We reasoned these non-HS-regulated genes have functions too important for basic survival to tolerate large stress-associated expression-changes, and these genes were not considered drivers of the HS-response. We identified 94 genes significantly upregulated in HS across all three parasites (↑↑↑), which were functionally enriched for protein-folding, chaperone-related processes, and other processes related to heat-stress and the UPR, in agreement with previous expression-based studies [5], as well as enrichment-results from HS-Sensitive mutants in our pooled screening, indicating the parasite increases production of heat-shock proteins (HSPs) and associated chaperones to repair the glut of proteins damaged/misfolded by heat-stress (Table S3B-D). Energy-producing processes (gluconeogenesis, glycolysis) were also upregulated, suggesting the parasite reroutes anabolic metabolism to increase

energy production to support ATP-dependent processes such as protein-refolding to correct heat-damaged proteins. Genes upregulated in HS were further enriched for processes involved in host-cell remodeling, including genes targeted to the Maurer's clefts, the host cell, and intracellular vesicles—all known to be important for parasite-remodeling of the host-cell to promote structural reinforcement against heat-shock damage to ensure its own survival [4, 5]. Organellar targeting to the mitochondria and apicoplast are also enriched in upregulated HS-responsive genes. The parasite's increased utilization of mitochondrial stress-response pathways may aid in degrading heat-damaged proteins that cannot be correctly refolded. Increased activity in the food digestive vacuole may allow the parasite to phagocytose and eliminate toxic misfolded protein-aggregates. The apicoplast involvement, particularly the isoprenoid biosynthesis pathway, has not been previously implicated in the HS-response.

Genes downregulated in all three parasites in response to HS (↓↓↓, n = 205) were enriched for virulence-factor and invasion-machinery-associated GO terms, suggesting the parasite decreases production of transcripts associated with pathogenesis, invasion and egress, lengthening its intracellular recovery-time to address global protein-damage.

Both HS-Sensitive mutants share many characteristic features of the wildtype response to febrile temperatures, which likely enabled their survival (Fig. 3A-B, red, blue; Table S3C-D). We identified two primary expression categories of genes dysregulated in the HS-Senstive mutants: (1) genes upregulated in the wildtype HS-response that were otherwise dysregulated in the HS-Sensitive mutants, which we interpreted as loss-of-function changes (↑⤮⤮, n=83), and (2) genes that were not regulated in response to HS in the wildtype but were upregulated in the HS-Sensitive mutants (– ↑↑, n = 74),

presumably equivalent to dominant-negative gain-of-function changes (Fig. 3A-B, ochre and tan, respectively). This first category of mutant-dysregulated genes (↑↗↗) was enriched for the UPR, as well as mitochondrial and apicoplast-localized pathways (cytochrome oxidase-assembly and fatty-acid biosynthesis, respectively). Several apicoplast isoprenoid biosynthesis-related genes upregulated in the wildtype HS-response were additionally dysregulated in one or both HS-Sensitive *pB*-mutant clones (Fig. 3C). The second category of mutant-dysregulated genes (– ↑↑), those that are not HS-responsive in wildtype, were enriched for translation-associated processes.

These data taken together suggest underlying mechanisms responsible for the HS-response. Critically, HS-Sensitive mutants fail to upregulate mitochondrial and apicoplast stress-response pathways, as well as signal peptide-processing pathways that might enable appropriate activation of those pathways. Mutants do not increase production of transcripts associated with responding to unfolded proteins. HS-Sensitive mutants additionally upregulate translation-related processes in response to HS when translation should be paused or neutral. This increase may overwhelm the parasite's capacity to repair or degrade heat-damaged proteins, exacerbating the formation/accumulation of toxic misfolded-protein aggregates that increase parasite sensitivity to HS.

Apicoplast isoprenoid biosynthesis is critical for *P. falciparum* survival of febrile temperatures

We examined our RNAseq data more closely to discern contributions of the apicoplast to HS-survival (Fig. 4A-E; Table S4A-D). We found that apicoplast-targeted genes tended to be increased in response to HS as compared to all non-apicoplast-targeted genes (Fig. 4A), were more likely to be essential during ideal blood-stage growth conditions

(Fig. 4B), were enriched for stress-response processes such as the UPR and oxidative-stress, and less expectedly, isoprenoid biosynthesis (Fig. 4C). As a major function of isoprenoid biosynthesis is in protein-prenylation—an important post-translational modification that regulates protein-targeting and function throughout the cell—we hypothesized that mutants in known-prenylated proteins [17, 18] would also have a phenotype in HS. We examined our 1K mutant-library for representation of isoprenoid biosynthesis, its immediate upstream-regulators (proteins responsible for modulation and import of glycolytic intermediates that serve as pathway substrates), and immediate downstream-effector proteins, and found that all eight isoprenoid biosynthesis-related *pB*-mutants included in the pooled screen were indeed HS-Sensitive (Fig. 4D, Table S4C).

Based on these data we further hypothesized that proteins or pathways allowing *P. falciparum* survival of febrile temperatures would be absent or otherwise divergent in *Plasmodium* species whose hosts do not mount fever-responses. We therefore compared the apicoplast isoprenoid biosynthesis pathway between *P. falciparum* and two rodent-infective species, *P. berghei* and *P. yoelii*. We found key thiamine-synthesis enzymes directly upstream of the pathway missing in the rodent-infective malaria parasites, including hydroxy-ethylthiazole kinase (ThzK); ThzK is up-regulated in the canonical parasite response to febrile temperatures and dysregulated in HS-Sensitive mutants (Fig. 4E, Table S4C-D). Perhaps most importantly, DOXP-Synthase (DXS), the critical enzyme marking the first step in isoprenoid biosynthesis, is upregulated in HS, dysregulated in HS-Sensitive mutants, and was HS-Sensitive in pooled screening, as were all four members of the prenylated blood-stage proteome represented in our screen (Fig. 4E, Table S4C-D). These data taken together strongly implicate isoprenoid biosynthesis in the HS-response.

Though the apicoplast has not previously been implicated in parasite survival of febrile temperatures, there is extensive literature on the ability of plants to mount effective defenses against heat as well as other external stressors, particularly critical for non-motile organisms at the mercy of their environments. We investigated the relationship between the parasite's HS-response and "plant-like" stress-responses by evaluating phyletic distribution of parasite HS-response genes in representative plant and algal genomes. *P. falciparum* genes with plant orthologs indicating potential endosymbiont-ancestry tended to be increased in response to HS vs. genes that do not have plant orthologs (Fig. 4F). These lines of evidence considered together present an evolutionary explanation that endosymbiosis of the apicoplast's algal progenitor enabled parasite-survival of extreme temperatures.

Processes enabling parasites to survive fever also drive resistance to artemisinin

We noted similarities between processes we identified to be driving the parasite HS-response and those implicated in parasite-resistance to artemisinin [7, 8, 10]. Therefore, we did a series of parallel phenotype-screens of our *pB*-mutant pilot-library using sublethal concentrations of two artemisinin compounds (dihydroartemisinin, DHA; artesunate, AS), heightened conditions of oxidative stress of RBCs, and exposure to a proteasome inhibitor (Bortezomib; BTZ) to investigate the possible relationship between HS-response and artemisinin MOA, as well as Oxidative-Screens (Fig. 5A, Table S5, Fig. S2A, Methods) . We found that HS-Sensitive mutants tended to be sensitive to both artemisinin derivatives and H_2O_2-induced oxidative stress, while HS-Tolerant mutants were less sensitive to either condition (Fig. 5A). Also, HS-Sensitive mutants shared an increased sensitivity to the proteasome inhibitor BTZ, consistent with laboratory observations connecting artemisinin MOA to the proteasome and clinical data that

362 proteasome-inhibitors act synergistically with artemisinins [8, 19, 20, 21]. Overall, correlation
363 of mutant phenotypic profiles across screens varied, with 16-45% having correlating
364 phenotypes in at least one additional screen (Fig. 5B, Fig. S2B).
365
366 We next assessed whether these laboratory-based experimental findings corresponded
367 to 'real world' changes associated with *P. falciparum* in artemisinin-resistant (ART-R)
368 clinical isolates [10]. Consistent with our laboratory findings linking HS-sensitivity and
369 ART-sensitivity, we found that genes mRNA levels of HS-Sensitive genes are
370 significantly positively correlated with parasite clearance half-life under treatment with
371 artemisinin-based combination therapies in recent field-isolates compared with HS-
372 Tolerant genes[10] (Fig. 5C, Tables S2 and S6). We also compared genes by HS-
373 response expression category to mRNA expression levels in these field isolates, finding
374 that genes upregulated in response to heat stress are significantly positively correlated
375 with parasite clearance half-life, while genes downregulated in response to heat stress
376 are more likely to be negatively correlated (Fig 5D, Tables S3 and S6). Therefore, we
377 conclude the parasite's responses to heat shock mirror the responses to artemisinin as
378 both are similar types of cellular stress on the parasite. Both of these stressors induce
379 unfolded protein responses, which include both upregulation and down regulation of
380 metabolic activities that enable the parasite to tolerate the toxic effects of accumulating
381 damaged proteins. The upregulated processes include the proteasome core and
382 chaperones to degrade or refold damaged proteins, while many other aspects of
383 metabolism, including growth-related anabolic processes, are down regulated to prevent
384 build-up of new proteins that may be damaged.
385
386 Artemisinin is activated by degradation of host hemoglobin. Recent evidence has
387 suggested two key, temporally-distinct ART-R mechanisms: (1) a multi-functional protein

388 long associated with resistance in field-isolates, *kelch13* (K13) confers resistance
389 upstream of hemoglobin degradation by modulating an associated endocytosis pathway;
390 and (2) downstream of hemoglobin degradation through the ubiquitin-proteasome
391 system (UPS), where K13 may function as or regulate a ubiquitin ligase [10, 11, 12, 22, 23, 24, 25].
392 In upstream-resistance, endocytotic transport of hemoglobin to the digestive vacuole
393 (DV) is down-regulated as this is the key process through which the parasite ingests,
394 degrades, and then releases hemoglobin. K13 mutant-isolates appear to downregulate
395 processes along this endocytosis pathway, decreasing parasite hemoglobin digestion
396 and release of heme to activate artemisinin, thereby increasing parasite survival. We
397 found that K13-defined endocytosis is also downregulated in response to HS (Fig. 5E).
398 As the K13-mediated endocytosis pathway culminates in host haemoglobin-cargo being
399 degraded in the DV, we further assessed our 1k HS-screen for DV-associated proteins.
400 We found DV-associated proteins did tend to be sensitive to heat-shock, including key
401 DV resident-proteases (Plasmepsin I, M1-family alanyl aminopeptidase; Fig. S3A) [26]. We
402 next evaluated our 1K-library HS-Screen for direct K13-interacting partner-proteins
403 recently identified via immunoprecipitation [25], and found that mutants in 10 of the 24
404 unique putative K13-partner-proteins represented in the screen were sensitive to HS.
405 Further, 5 of 7 known alkylation-targets of artemisinin represented in our screen had
406 sensitivity to HS [9, 26] (Fig. S3B). We noted significant overlap in each of these categories
407 of ART MOA-related genes and isoprenoid biosynthesis-related genes (Fig. S3C).
408
409 In a second downstream step post-activation of artemisinin, the parasite engages the
410 UPS to further mitigate artemisinin-induced damage. Artemisinins mount a multi-pronged
411 attack against the parasite by causing a global, non-specific accumulation of damaged
412 parasite proteins, which are then polyubiquitinated/marked for degradation, while also
413 inhibiting proteasome-function. These poly-ubiquitinated proteins ultimately overwhelm

414 the parasite's decreased capacity for UPS-mediated protein-degradation [8]. Key
415 ubiquitinating components of this system, including E2/E3 ligases and K13, are
416 downregulated in response to HS, while key components of the UPR and protein folding
417 are increased (Fig. 5E). In contrast, components of the core proteasome were
418 universally increased in response to HS when considered in aggregate, although the
419 change did not meet our fold-change criteria for being HS-regulated (Fig. S4A).
420
421 Synthesizing these data, we present a model for the relationship between what is
422 currently understood of artemisinin MOA and HS-response (Fig. 5F). The canonical
423 parasite-response to fever is to increase protein-folding and UPR while inhibiting
424 ubiquitination to prevent accumulation of toxic, polyubiquitinated protein-aggregates. The
425 parasite simultaneously increases its capacity for proteasome-mediated degradation—
426 ultimately enabling it to resolve HS-instigated stress and thus survive febrile
427 temperatures (Fig. S4B). As heat-stress is also injurious to the host RBC, the parasite
428 diverts resources to stabilize the host cell—increasing export and trafficking of proteins
429 involved in host-cell remodeling that support fortification of the host-cell membrane, as
430 well as decreasing uptake of host-cell hemoglobin through the K13-mediated
431 endocytosis pathway—processes which are ultimately driven by prenylation downstream
432 of apicoplast isoprenoid biosynthesis. Artemisinins kill by overwhelming these same
433 pathways: damaging and unfolding proteins, preventing folding of newly synthesized
434 proteins and inhibiting the proteasome, while at the same time activating ubiquitination-
435 machinery to ensure the accumulation of toxic polyubiquitinated proteins that eventually
436 cause cell-death. ART-R-associated mutations allow the parasite to constitutively
437 activate unfolded-protein response mechanisms which increase its capacity for refolding
438 or degrading those toxic proteins [27]. The overall increase in damaged-protein
439 degradation-capacity allows ART-R parasites to keep up with the influx of artemisinin-

induced protein-damage, clearing the waste and enabling parasite survival. This direct inverse relationship in activation of endocytosis, the ubiquitin-proteasome system and other pathways underlying DHA-mediated killing and febrile-temperature survival, supports a shared mechanism for artemisinin-resistance and HS-response, suggesting that ART-R parasites evolved to harness canonical HS-survival mechanisms to survive artemisinin.

Discussion

Our data indicate that the parasite crisis-response to HS is multi-faceted to relieve the build-up of heat-damaged proteins before it is overwhelmed by toxic, misfolded-protein aggregates. Responding to or perhaps preventing a build-up of potentially toxic heat-damaged proteins, the parasite upregulates expression of chaperones to stabilize and detoxify them, downregulating ubiquitinating enzymes to discourage their aggregation while upregulating the core proteasome and vesicular trafficking to degrade and eliminate proteins which can't be repaired. Equally important in the survival-response are changes in redox homeostasis, lipid metabolism, cellular transport, and metabolic processes associated with the endosymbiont-derived organelles. The parasite requires increased energy to mount this febrile response, which it provides by redirecting its own internal biosynthetic pathways to produce glucose. Interestingly, we confirm the parasite's protective response-mechanisms include proteins exported into the erythrocyte, suggesting that the parasite's metabolic processes exported to remodelled cytoplasm of the parasitized host cell are equally vulnerable and vital to malaria parasite survival.

The apicoplast genes have a higher proportion of up-regulated genes in HS and tend to be essential under normal growth situation. (Fig. 4A,B). The apicoplast isoprenoid

466 biosynthesis pathway's critical involvement in survival of febrile temperatures is
467 nevertheless a surprise, as it has not been implicated before in the *Plasmodium* HS-
468 response. Isoprenoids are required for myriad functions across the tree of life—plant
469 chloroplasts, algae, some parasitic-protozoa and bacterial pathogens utilize a
470 specialized form of this pathway absent from all metazoans (also called the MEP or
471 DOXP non-mevalonate pathway), which has made isoprenoid biosynthesis an attractive
472 target for intervention against a range of pathogens [28, 29]. Most studied organisms make
473 wide use of protein-prenylation and have large prenylated proteomes; malaria parasites,
474 in contrast, have a very small prenylated blood-stage proteome (~20 proteins) consisting
475 primarily of vesicular trafficking proteins, notably the Rab-family GTPases [17, 18]. Recent
476 studies indicate the key essential function of isoprenoids in the parasite blood-stage is in
477 their roles as substrate for protein-prenylation—specifically, in prenylating proteins
478 driving vesicular transport to the digestive vacuole [30, 31]. In the absence of prenylation,
479 Rab5 trafficking is disrupted, which leads to digestive vacuole-destabilization and
480 parasite death [31]. Notably, artemisinin also disrupts digestive vacuole-morphology,
481 resulting in a very similar phenotype as a consequence of its activation via hemoglobin
482 digestion [32, 33]. Intriguingly, recent data confirm the association of key resistance-
483 mediator K13 with Rab-GTPases [25], adding to the repertoire of proteins comprising K13-
484 mediated endocytic vesicles, and by extension supporting the role of prenylation in K13-
485 mediated processes associated with ART MOA.
486
487 Another key parasite-defense against oxidative stress induced by pro-oxidant
488 compounds (such as artemisinin) includes increased vitamin E biosynthesis—another
489 exclusive function of the MEP isoprenoid-biosynthesis pathway, whose stress-related
490 regulation has been extensively studied in plants [34, 35]. Further insights to the role
491 isoprenoids play in the HS-response may be gleaned from plants and pathogenic

492 bacteria, where research suggests key branchpoint-enzyme DXS, which catalyzes the
493 first and rate-determining step of the MEP pathway [36] has a role in sensing and then
494 facilitating adaptation to ever-changing environmental conditions, including temperature,
495 light-exposure, chemical compounds, and oxidative stress (for example [37, 38]). Elevated
496 levels of isoprenoids have been found to correlate with plant exposure to drought and
497 other stressors and are considered a key component of plant-defenses against abiotic
498 stress [39]. The DXS ortholog may play a similar role in *P. falciparum*, enabling the
499 parasite to mount quick responses to unfavorable conditions in the host-environment,
500 such as fever.
501
502 Interestingly, concurrent studies now provide mechanistic insights illuminating the
503 biochemical relationship between apicoplast isoprenoid biosynthesis and the parasite
504 febrile-temperature survival response[40]. Farnesylation of HSP40 (PF3D7_1437900), a
505 type of prenylation mediated by the MEP pathway, is critical for *P. falciparum* survival of
506 thermal stress. In this study Inhibition of isoprenoid biosynthesis ultimately resulted in
507 reduced association of HSP40 with critical components of the cytoskeleton, protein-
508 export, and vesicular transport pathways—without which *P. falciparum* could survive
509 neither heat nor cold stress. Suppression of these cellular processes by loss of HSP40-
510 farnesylation directly corresponds to HS-sensitive pathways identified via both our
511 forward-genetic screen and our gene-expression analyses of the HS-Sensitive LRR5-
512 and DHC4-mutant clones.
513
514 Few eukaryotes are known to be able to thrive in extreme-heat environments; most are
515 unable to complete their lifecycles above 40°C [41]. The survival mechanism of malaria
516 parasites could be attributed to the algal ancestral lineage of the apicoplast. Some
517 extant red algal-lineages (genus *Cyanidioschyzon*) are extremophilic inhabitants of

518 acidic hot-springs and are remarkably resistant to heat shock up to 63°C; green-algae
519 *Chlamydamonas reinhardtii* was also able to survive to 42°C [42]. Responsibility for this
520 extreme resistance to transient exposure to high temperatures was attributed to two
521 genes of the small heat shock protein (sHSP) family (CMJ100C and CMJ101C). The *P.*
522 *falciparum* ortholog for these genes (PF3D7_1304500) was upregulated in the wildtype
523 HS-response and dysregulated in both our HS-Sensitive mutants, indicating its
524 contribution to parasite survival in extreme temperatures. Mutations in this gene were
525 not represented in our pooled screens.
526
527 It is tempting to speculate that presence of the endosymbiont cynobacterium-related
528 ancestral genes and its associated plant stress-response mechanisms is what enabled
529 the ancestral parasite to survive host-fever, likely an important and early step leading to
530 successful infection of hominid hosts. Our findings of significant overlap between
531 parasite-responses to three disparate stressors (HS, artemisinin, oxidative stress) offers
532 new insight into how *P. falciparum* exhibited artemisinin-resistance even in the initial
533 clinical trials [43], and then further evolved resistance relatively quickly after mass-
534 introduction of the drug by “hijacking” and repurposing the parasite's in-built fever-
535 response pathways.
536
537 **Conclusion**
538 Deeper knowledge of parasite biology is expected to enable more effective and likely
539 longer-lasting antimalarial interventions. Similarly, a better mechanistic understanding of
540 artemisinin MOA will lead to better combination therapies to combat emerging
541 resistance. With this first large-scale forward-genetic screen in *P. falciparum*, we
542 revealed the parasite’s survival responses to malarial fever and artemisinin

chemotherapy share common underpinnings that heavily depend on metabolic processes of plant origin.

ART-R ultimately hinges on highly efficient protein-degradation mechanisms. This mechanistic knowledge allows for the application of intelligently considered counters to ART-R, such as combinatorial therapy with proteasome-inhibitors, which has experimentally shown great promise [44]. Our current study highlights the potential of forward-genetic screens to elucidate unexpected processes and pathways, such as DOXP and isoprenoid biosynthesis, that are associated with the artemisinin MOA which may serve as synergistic druggable targets [45]. Future studies can exploit a genome-wide screening approach to iteratively ascribe function to every part of the malaria-parasite genome to support targeted development of new, more-efficacious antimalarial combination therapies to limit and potentially reverse artemisinin resistance.

Declarations

Ethics approval and consent to participate

Not applicable.

Consent for publication

Not applicable.

Availability of data and materials

The raw RNAseq dataset supporting the conclusions of this article are available in the Mendeley Data repository *Malaria-parasite survival of host fever is linked to artemisinin resistance*, http://dx.doi.org/10.17632/b8g3wbnd5v.1 [46]. Raw QIseq dataset accession numbers are listed in Table S5.

Competing interests

The authors declare that they have no competing interests.

Funding

This work was supported by the National Institutes of Health grant R01 AI094973 and R01 AI117017 (J.H.A.) and the Wellcome Trust grant 098051 (J.C.R.).

Authors' contributions

Conceptualization, M.Z., C.W., J.O., T.D.O., J.C.R., M.T.F., R.H.Y.J., and J.H.A.; Methodology, M.Z., C.W., J.O., K.B.S., R.H.Y.J., and J.H.A.; Software, J.O. and C.W.; Validation, M.Z., C.W., and J.O.; Formal Analysis, M.Z., C.W., J.O., S.R.A., and R.H.Y.J.; Investigation, M.Z., C.W., J.O., P.T., D.C., S.B., S.X., M.M., and R.H.Y.J.; Data Curation, M.Z., C.W., and J.O.; Writing—Original Draft, J.O., M.Z., and J.H.A.; Writing—Review & Editing, J.O., M.Z., T.D.O., J.C.R. and J.H.A.; Visualization, C.W., M.Z., J.O., and R.H.Y.J.; Supervision, M.Z., J.O., T.D.O., J.C.R., M.T.F., R.H.Y.J., and J.H.A.; Project Administration, M.Z.; Funding Acquisition, J.C.R. and J.H.A.

Acknowledgements

We appreciate the Wellcome Sanger Institute (United Kingdom) for performing QIseq and Xiangyun Liao, Suzanne Li, and Kenneth Udenze for support of parasite cell culture. We thank the USF Genomics Program Omics Hub for productive discussion.

FIGURE LEGENDS

Figure 1. Pooled screens of *P. falciparum piggyBac* mutants allow robust identification of heat-shock phenotypes. A. Experimental design for pooled heat

shock (HS) phenotypic screens. The pilot-library of *pB*-mutant clones (n=128) was exposed to three rounds of temperature-cycling (41°C for 8 hours) to simulate malarial fever (Methods, Pooled-screen assay-design). A pilot-library control concurrently grown continuously at 37°C established inherent growth of each *pB* mutant. HS screens of the pilot-library were conducted in biological duplicate and technical triplicate and were highly correlated, indicating high accuracy and reproducibility (See Fig. S5A; Methods, Pooled-screen assay-design, HS-Screen).

B. QIseq quantifies each *pB*-mutant in the pilot-library from sequence-reads of the 5′ and 3′ ends of each *pB* insertion-site. Colored lines represent genes. Black boxes indicate transposon location (Fig. S5B; Methods, QIseq).

C. Pilot-library mutant growth-phenotypes at ideal temperatures, defined as fold change in QIseq reads-count after three cycles growth at 37°C (FC-Growth; Methods) ranked from Sensitive to Tolerant. Mutants with inherently slower or faster growth under ideal conditions are shown in grey and blue, respectively.

D. Pilot-library mutant HS-phenotypes ordered from Sensitive (red) to Tolerant (green). Mutant growth was defined as QIseq reads-count fold-change in response to HS (FC-HS) vs. non heat-shocked control (Methods). HS-Sensitive mutants have lower FC-HS (red, FC-HS < 1), while HS-Tolerant mutants have higher FC-HS (green, FC-HS > 1).

E. HS- and Growth-phenotypes of the pilot-library mutants. HS-phenotype of each mutant (displayed as line-graph) is superimposed on its corresponding Growth-phenotype (bar graph). *Known HS-Sensitive and **HS-Tolerant pB-mutant clones served as benchmarks in the pilot-library HS-Screen for identifying sensitive/tolerant mutants [15].

F. Phenotype-comparison between mutants characterized in both individual HS-assays[15] and pooled HS-screening (n = 20). Mutant clones without an observed phenotype in individual HS-assay as determined by above-average growth via flow cytometry (green)

also had significantly higher Phenotypic Fitness Scores in response to HS (PFS_{HS}) in pooled screening, while mutant clones characterized as HS-Sensitive in individual assays (red) also had significantly lower PFS_{HS} in pooled screening. (** p-value < 0.01, Mann-Whitney U test),

G. Mutant heat-shock phenotype classifications. Red = HS-Sensitive mutants (FC-HS < 0.5 and PFS_{HS} < 0.25, n = 28). Yellow = mutants classified as both Growth-Sensitive and HS-Sensitive (FC-HS < 0.5, PFS_{HS} > 0.25, n = 14). Green = HS-Tolerant mutants (FC-HS > 1.5, n = 30). Mutants neither Sensitive nor Tolerant to HS were classified as HS-Neutral (n = 49) (Methods) .

H. Distributions of PFS_{HS} for mutant HS-phenotype classifications. HS-Sensitive mutants are assigned the lowest PFS_{HS}, while HS-Tolerant mutations are assigned the highest PFS_{HS} (**** Wilcoxon-test p-value < 1e-15).

Figure 2. Large-scale pooled phenotypic screens enable identification of processes driving the *P. falciparum* heat-shock response.

A. HS-Sensitive mutations identified in pooled screens of 1K-library of 922 *pB*-mutants (Table S2). The uncloned, large mixed-population pools comprising the 1K-library (n = 10) were parallely screened in both ideal growth conditions and under HS, and mutants were assigned phenotypes as per methods established in the pilot-library screens (Fig. 1, Table S1, Methods). Mutants are ranked by fold-change in response to HS from HS-Sensitive (red; n = 149, FC-HS < 0.5 and PFS_{HS} < 0.25) to HS-Tolerant (green; n = 139, FC-HS > 1.5). Mean mutant fold-change in ideal growth (FC-Growth) is superimposed as a bar plot (gray, FC-Growth < 1.0; blue, FC-Growth > 1.0). Mutants performing poorly in both screens (yellow; n = 91, FC-HS < 0.5, PFS_{HS} > 0.25) were classified as HS- and Growth-Sensitive and were not considered further. Mutations neither HS-Sensitive nor HS-Tolerant were classified as HS-Neutral (taupe, n = 543). The distribution patterns

between intergenic regions and CDS is almost equal comparison of pilot-library and 1K-library that demonstrate the random nature of the *pB*-mutant library (Fig. S6A-C). We checked reproducibility and validate the performance of the 1K- library by comparing correlation of the *pB*-mutants that appeared multiple times (i.e., at least twice) in different pools (Fig. S7A-B). In addition to the HS-Sensitive mutant PB4 (DHA, dynein, PF3D7_1122900) from the pilot library, we identified three HS-Sensitive dynein mutants in the 1K-library (two different mutants of DHA_12, PF3D7_1202300; one mutant of DHA_10, PF3D7_1023100), indicating the robusticity of the 1K-library screen (Fig. S8A-B). Distributions of PFS_{HS} for mutant HS-phenotype classifications are provided in Fig. S9.

B. Functional enrichment of GO terms for HS-Sensitive or Growth-Sensitive *pB*-mutants vs all other mutants in the 1K-library. HS-Sensitive mutants were enriched in terms associated with HS-response such as protein-folding, response to DNA-damage, DNA-repair, and regulation of vesicle-mediated transport. Growth-Sensitive mutants tended to be enriched for more general categories broadly important for survival in all conditions, such as translation- or mRNA-metabolism-related terms. Circles represent GO category, circle color represents ontology, and circle size represents number of significant genes annotated to that category. Significant terms (Fisher/elim-hybrid test p. value <= 0.05) fall within the light-green box.

Figure 3. Unfolded protein response, apicoplast-targeted and mitochondria-targeted stress-response pathways are critically dysregulated in functionally unrelated HS-Sensitive mutant clones.

A. Genes were classified based on their NF54-expression with and without HS-exposure across all three parasite lines (Table S3, Methods). Genes identified as differentially expressed in response to febrile temperatures vs. 37°C were classified into three

different categories based on direction of response in the wildtype parasite NF54: upregulated in response to HS (FC-HS > 1 and FDR < 0.1; ↑ n=415), down-regulated in response to HS (FC-HS < -0.5 and FDR < 0.1;↓ n=611), or not regulated by HS (-0.5 < FC-HS < 1; – n=1541), with upregulated genes considered to be driving the HS-response. Genes expressed above threshold in NF54 and both HS-Sensitive mutants (n = 1298) were then assigned into six HS expression-categories based on phenotype in NF54 vs. mutants *ΔLRR5* and *ΔDHC*. HS-regulated genes shared between NF54 and both mutants are indicated in red (↑↑↑, n = 94) or blue (↓↓↓, n = 205) for up- and down-regulated genes, respectively. Genes dysregulated in one or both HS-Sensitive mutants fell into two main expression-profile categories underlying mutant HS-Sensitivity phenotypes: those upregulated in NF54 that failed to be regulated in the mutants (↑⇗⇗, n = 83), and genes not regulated in response to HS in NF54 that were inappropriately upregulated in the mutants (– ↑↑, n=74). Most remaining genes were not regulated in response to HS in any parasite line (n = 615).

B. Functional enrichment analyses between wildtype/mutant HS-expression profiles as defined in A. Red: Shared upregulated HS-responsive GO-terms between NF54 and the two HS-Sensitive *pB*-mutants (↑↑↑). Blue: Shared down-regulated HS-responsive GO-terms (↓↓↓). Ochre: GO-terms upregulated in NF54 but dysregulated in the two *pB*-mutant (↑⇗⇗). Tan: GO-terms enriched in genes not regulated in the wildtype HS-response but upregulated in the mutants (– ↑↑). Only enriched GO-terms are shown (Fisher/elim-hybrid test p. value <= 0.05), with highest significance indicated in dark green. Fraction of significant genes mapping to a GO-term in an HS expression-profile category vs. genes mapping to that GO-term in the entire analysis is indicated by distance to the center of the circle, with the outermost position on the circle indicating 100% of genes in that GO-term are significant. See Table S3D.

C. Several apicoplast and isoprenoid biosynthesis-related genes have a tendency to be upregulated in the wildtype-response to HS and are dysregulated in one or both HS-Sensitive *pB*-mutant clones (↑⇗⇗). * Isoprenoid biosynthesis-related genes upregulated by HS confirmed in the pooled HS-Screen.

Figure 4. Apicoplast isoprenoid biosynthesis is critical for *P. falciparum* survival of febrile temperatures. A. Apicoplast-targeted genes tend to be increased in response to HS as compared to all non apicoplast-targeted genes detected above threshold in RNAseq. Apicoplast-targeted genes are as defined in [47] (*** Fisher-test p-value < 1e-5, 39 up- vs.12 down-regulated genes, compared with whole genome 415 up- vs. 611 down-regulated genes, Fisher test p< 1e-5, Table S4A-B).
B. Apicoplast-targeted genes tend to be highly essential during blood-stage vs. all other non-apicoplast-targeted genes detected above threshold in RNAseq. The lower Mutagenesis Index Score (MIS) represents higher essentiality [6], the median MIS for apicoplast-targeted genes is much lower than median MIS for all other genes, indicating a lower tolerance for disruption and thus higher likely essentiality during blood-stage development than non-apicoplast-targeted genes (**** Wilcoxon-test p-value < 1e-15).
C. Apicoplast pathways regulated in response to HS. GO categories enriched in up- and down-regulated apicoplast genes are shown on a scale from red to blue, respectively. The horizontal direction indicates the log ratio between up- and down-regulated apicoplast genes in each category. Circle-size represents gene-number per category.
D. All nine *pB*-mutants in genes related to apicoplast isoprenoid biosynthesis represented in the 1K-library pooled screen were HS-Sensitive. Mutants are ranked by phenotype from HS-Sensitive (red) to HS-Tolerant (green). Circles indicate each HS-Sensitive mutant related to isoprenoid-biosynthesis. *The three isoprenoid biosynthesis-

genes we identified as directly upregulated in response to HS via RNAseq (DXS, PF3D7_1337200; tRNA m(1)G methyltransferase, PF3D7_1119100; apicoplast RNA methyltransferase, PF3D7_0218300). See Table S3.

E. Key enzymes in the *P. falciparum* isoprenoid biosynthesis-pathway are up-regulated in response to heat-shock (red circle), dysregulated in HS-Sensitive mutants (ochre) and absent in malaria-parasites of hosts that do not present fever. Pathway diagram modeled from [48]. Isoprenoid biosynthesis-genes upregulated in HS include DXS, 2-C-methyl-D-erythritol 2,4-cyclodiphosphate synthase (IspF, PF3D7_0209300), pyruvate kinase II (PyKII, PF3D7_1037100), phosphoenolpyruvate/phosphate translocator (PPT, PF3D7_0530200), triosephosphate isomerase (TIM, PF3D7_1439900), triose phosphate transporter (TPT, PF3D7_1218400), and upstream-regulator of MEP-pathway substrates HAD1-phosphotase (HAD1, PF3D7_1033400) [49]. All direct downstream-targets prenylated by bifunctional farnesyl/geranylgeranyl diphosphate synthase (FPPS/GGPPS, PF3D7_1128400) with products of the MEP-pathway (zigzag) represented in pooled screening were HS-Sensitive, including the Rab-family vesicular trafficking-proteins (Rab5c, PF3D7_0106800; Rab7, PF3D7_0903200; Rab11b, PF3D7_1340700), as were several digestive vacuole proteases and proteins involved in hemoglobin digestion (PM1, PF3D7_1407900; ATCase, PF3D7_1344800; M1AAP, PF3D7_1311800; LAP, PF3D7_1446200; HSP70, PF3D7_0818900). The key thiamin-synthesis enzyme hydroxyethylthiazole kinase (ThzK, PF3D7_1239600) is absent in *P. berghei* and *P. yoelii*, malaria-parasites whose rodent-hosts do not present fever.

F. *P. falciparum* genes with plant orthologs (green circles) indicating potential endosymbiont-ancestry tend to be increased in response to HS vs. genes that do not have plant orthologs (grey circles). *P. falciparum* genes with potential endosymbiont-ancestry were derived from 1919 ortholog-pairs between *Arabidopsis thaliana* and *P.*

748 *falciparum* (data from OrthoMCLv5.0). The listed processes are sorted based on the
749 ratio of “green” to “non-green” orthologs.
750
751 **Figure 5. Increased sensitivity to fever is directly correlated with increased**
752 **sensitivity to artemisinin in the malaria parasite. A.** HS-Sensitive *pB*-mutants (red)
753 are more sensitive to multiple concentrations of artemisinin derivatives Artesunate (AS)
754 and Dihydroartemisinin (DHA), proteasome-inhibitor Bortezomib (BTZ), and conditions of
755 heightened oxidative stress than HS-tolerant parasites (green) in all pooled screens of
756 the pilot library. HS-Sensitive mutants tended to be sensitive to both artemisinin
757 derivatives and H_2O_2-induced oxidative stress, while HS-Tolerant mutants were less
758 sensitive to either condition. Also, HS-Sensitive mutants shared an increased sensitivity
759 to the proteasome inhibitor BTZ (Table S5, Fig. S2, Methods). *pB*-mutants were cultured
760 continuously under oxidative stress-inducing conditions for three to six cycles (T1 and
761 T2, respectively). Samples were collected from all parallel phenotype-screens of the
762 pilot-library in biological duplicate. Biological replicates were highly correlated for each
763 screen (Pearson correlation > 0.94; Fig. S2 and S10). Mutants in apicoplast-targeted
764 genes (n = 5) have phenotypes similar to all HS-Sensitive mutants (n =28) in artemisinin-
765 derivative screens, but not to protein-inhibitors or oxidative stress (* Wilcoxon $p < 0.05$;
766 *** Wilcoxon $p < 1e\text{-}10$. See Methods).
767 **B.** Correlation between mutant phenotypes in all pooled screens of the pilot library.
768 Mutants performing in the bottom 25% or top 25% of each screen were classified as
769 having “Sensitive” and “Tolerant” phenotypes, respectively. Mutant classifications were
770 compared pair-wise between each screen, with mutants falling into the same category in
771 both screens considered to have correlating phenotypes.
772 **C.** Compared with HS-Tolerant genes, the mRNA levels of HS-Sensitive genes are
773 significantly positively correlated with parasite clearance half-life under artemisinin-

based combination therapy (ACT) in field-isolates[10]. The red violin plot indicates 29 HS-Sensitive *pB*-mutants, while the green violin plot represents 16 HS-Tolerant mutants (* Wilcoxon p-value < 0.05).

D. Under HS stress, genes classified as up-regulated in response to heat-stress are significantly positively correlated with parasite clearance half-life under artemisinin-based combination therapy (ACT) in field-isolates[10]. Down-regulated genes are more likely to be negative correlated with parasite clearance half-life. The red violin plot indicates 67 genes upregulated in WT during HS, while 114 genes are down-regulated (** Wilcoxon p-value < 1e-3).

E. Both K13-mediated mechanisms of artemisinin resistance (endocytosis, ubiquitin-proteasome system) are similarly regulated in HS. The K13-defined endocytosis pathway (shades of green) and key ubiquitinating-enzymes of the ubiquitin-proteasome system, E2/E3 and K13, are downregulated in the wildtype NF54 HS-response, while protein folding, stress, exported proteins, and proteasome genes are upregulated. RNAseq data are plotted for each gene by average log2 fold-change in response to HS and significance (–log2(p-value)). Circles in shades of blue and pink indicate genes significantly down- or upregulated after exposure to HS, respectively.

F. Proposed model integrating key pathways underlying the parasite survival of host fever-response and artemisinin resistance identified via pooled phenotypic screening. Direction of regulation in response to HS is informed by comparative RNAseq data where available (pink = increased; blue = decreased). Pathways/proteins previously identified as interacting with K13 are indicated (green triangle). See Tables S4C-D for data and additional supporting references.

Methods

Pilot-library of pB-mutant clones characteristics and validation

The single *piggyBac*-transposon insertion sites of each *pB*-mutant-clone in the pilot-library were verified as previously described [13, 14], published data showed that growth rates of individual *pB*-mutant clones were highly reproducible between biological replicates, and even between pools with different compositions. All of those 128 extensively characterized *P. falciparum pB*-mutant clones in the pilot-library were repeatedly confirmed in subsequent growth screens in 12 asexual intra-erythrocytic development cycles (24 days), bio-rep samples were collected in subsequent cycles at 3, 6, 9 and 12. Additionally, whole-genome sequencing performed on 23% of 128 *pB*-mutant-clones in the pilot-library verified that no major genomic changes occurred aside from the *piggyBac* insertion, ensuring any detected phenotypes are attributable to the single disruption [15]. The pilot-library was generated in a manner to ensure approximately equal representation of each of the 128 clones at thaw [13].

Generating the pilot-library of pB-*mutant parasite clones*

The pilot-library was built as described in our previous QIseq methods-development study [13] and data are available in PlasmoDB (RRID:SCR_013331). Aliquots of the pilot-library were generated by first growing each of the 128 extensively-characterized mutant-clones individually in T25-flasks to 1-2% parasitemia. All clones were then combined equally into one large flask and gently mixed. One-hundred equal-volume aliquots of the pilot-library were then cryopreserved according to standard methods, providing enough biological-replicate samples for use in the parallel phenotype screens of the pilot-library.

Pooled-screen assay-design

HS-screens

825 The pooled phenotypic screen-design pipeline has three important steps to ensure
826 quality-control and scalability: 1) protocols are tested using individual *pB*-mutant clones;
827 2) methods are adapted for pooled-screening using the well-characterized pilot-library;
828 3) methods developed using the pilot-library are applied to 1K-library screens (Fig. S1).
829 We exposed pools of *pB*-mutant parasites to three rounds of temperature-cycling to
830 simulate the cyclical pattern of fever characteristic of human malaria (Figure 1A).
831 Parasites under phenotypic selection (heat-shock) and ideal-growth controls originated
832 from the same thaw, grown at 37°C for one cycle then split equally into five flasks (three
833 flasks A, B and C for exposure to heat-shock, samples were harvested from these three
834 flasks at same time as three technical-replicates for HS-Screens; two flasks C and D for
835 the ideal-growth controls). Experimental and control-flasks were maintained in parallel to
836 minimize potential batch-effects. Parasites were grown for one cycle at 37°C until they
837 reached the ring-stage of development (Time-point 0; T^0), at which point the
838 experimental-group were exposed to febrile temperatures (41°C) for 8 hours. Post-heat-
839 shocked parasites were then returned to 37°C for the remainder of the 48-hour window
840 until they again reached ring-stage. Parasite-gDNA was harvested for QIseq after two
841 more rounds of temperature-cycling in successive growth cycles to ensure enough
842 parasite-material was available for QIseq (Time-point 1; T^1). Control-parasites were
843 harvested for gDNA before and after three cycles of pooled growth at 37°C (T^0 and T^1,
844 respectively) for quantification via QIseq in technical triplicate. We used QIseq-reads
845 obtained for each mutant after the same number of cycles of pooled growth at 37°C as
846 our T^0 control as previously reported [13]. Pilot-library screens were performed in biological
847 duplicate. As the 1K-library consists of multiple randomly selected, uncloned, large
848 mixed-population pools and direct biological replication is not feasible, we leveraged
849 insertions duplicated across pools as internal controls. FC-HS for 15 insertion-sites
850 represented in at least two different pools of the 1K library allowed evaluation of

851 consistency across pools. FC-HS was highly correlated between duplicate insertion-sites
852 regardless of the pool in which they were screened (Pearson correlation = 0.806; Fig.
853 S7A-B). We further evaluated reproducibility between the pilot library and the 1K library
854 using mutants in genes represented in both the pilot library and the 1K-library (n = 16
855 genes; max distance between pilot-library and 1K-library insertion < 1 kb). FC-HS was
856 again highly correlated across pools (Fig. S8A-B, Pearson correlation = 0.702).
857
858 *Drug-screens*
859 As with the HS-screen, parasites were split from the same thaw of the pilot-library after
860 one cycle of growth into experimental flasks and control-flasks. Experimental flasks were
861 exposed to three cycles of continuous drug-pressure at two different concentrations
862 (IC10, IC25) of each artemisinin-compound (AS, DHA). Proteasome-inhibitor BTZ-
863 experiments were performed at IC10. Control-flasks were cultured continuously in
864 parallel at 37°C without drug. Parasites were harvested immediately at the conclusion of
865 three growth-cycles for gDNA-extraction and phenotype-analysis via QIseq.
866
867 *Oxidative stress screens*
868 Parasites were split after one cycle of growth from the same thaw of the pilot-library as
869 the HS-screen. Parasites were grown one more cycle, then split into four flasks: two
870 control-flasks to be cultured with standard, washed human red blood-cells (hRBC), and
871 two experimental flasks to be cultured with H_2O_2-treated hRBCs to mimic conditions of
872 oxidative stress. Experimental flasks (H_2O_2 treated-hRBC) and control-flasks (untreated-
873 hRBC) were cultured continuously in parallel at 37°C. Parasites were harvested
874 immediately after three growth-cycles (T1), then again after an additional three growth-
875 cycles (T2) for gDNA-extraction and phenotype-analysis by QIseq.
876

Methods for oxidative pre-treatment of hRBCs were as published previously [50]. Briefly, O+ hRBCs (Interstate blood bank, packed, 100% hematocrit) were incubated with 1 mM H_2O_2 (Sigma-aldrich, Cat. no. H1009-100ML) for one hour at room temperature. After treatment, cells were washed three times with phosphate-buffered saline (PBS) before dithiothreitol (DTT) was added to a final concentration of 1 mM to heal any reversible oxidative damages. Cells were then treated with menadione sodium bisulphite for one hour at room temperature (Sigma-aldrich Cat. no. M5750-100G) and washed five times. A volume of 3–4 ml of AB medium (RPMI 1640 medium supplemented with 2 mM L-glutamine, 25 mM HEPES, 100 µM hypoxanthine and 20 µg ml^{-1} gentamicin) was added on top of the cell-pellet after discarding the final wash. Pre-treated erythrocytes were stored at 4 °C before use in parasite culture.

All pooled phenotypic screens of pilot-library (AS, DHA, BTZ, oxidative stress, ideal growth) were performed in biological duplicate (Fig. S10).

QIseq

QIseq, which uses Illumina next-gen sequencing technology and custom library-preparation to enable sequencing from both the 5' and 3' ends of the *piggyBac* transposon out into the disrupted genome-sequence, allows quantitative identification of each *pB*-mutant line by its unique insertion-site within mixed-population pools of *pB*-mutants [13] (Figure 1B). The anatomy of the *piggyBac* transposon and its distinct 5' and 3' inverted terminal-repeat sequences (ITRs) allows double-verification of insertion-sites; both 5' and 3' QIseq libraries were therefore generated and sequenced for each sample. Counts per insertion-site were determined as described previously [13]. We observed high correlation between biological replicates at 41C and 37C respectively (Pearson correlation = 0.964 at 41C and 0.967 at 37C, Fig. S5A). We observed lower correlation

903 between Growth (37C) and HS (41C) assays (Fig. S5B, average Pearson correlation =
904 0.723), suggesting that our heat-shock exposure-conditions are sufficient to allow
905 reproducible detection of mutants with specific selection response-phenotypes from
906 pooled screening.
907
908 *Calculating mutant fold-change in pooled screening to assign HS- and Growth-*
909 *phenotypes*
910 We defined FC-Growth by *pB*-mutant fold-change after three cycles of growth at ideal
911 temperatures ($T^{1\text{-}37C}$/ $T^{0\text{-}37C}$). FC-HS was defined as *pB*-mutant fold-change after
912 exposure to heat-shock vs. the non- heat-shocked control ($T^{1\text{-}41C}$/ $T^{1\text{-}37C}$). We used
913 changes in reads-number detected for each *pB*-mutant in the Growth-Screen and the
914 HS-Screen as compared to reads-number detected for that mutant in the respective
915 control-screen to calculate mutant Fold Change (FC) in both screens (Figure 1C-D;
916 Methods). We then ranked mutants from lowest to highest FC, with lowest FC indicating
917 highest sensitivity to the screened-condition.
918
919 We developed a scoring-system to distinguish mutants with phenotypes specifically in
920 the condition under selection (HS) vs. those with inherently compromised growth in ideal
921 conditions, called the Phenotypic Fitness-Score (PFS). PFS_{HS} is the mutant fold-change
922 in response to heat-shock (FC-HS, 41C/37C) multiplied by the ratio of FC-HS to mutant
923 fold-change under ideal growth-conditions (FC-HS/FC-Growth), with the smallest and
924 largest values indicating the largest mutant growth-differentials between the two screens
925 (smallest PFS_{HS} indicating worse mutant-fitness in the HS-Screen than the Growth-
926 Screen, and largest PFS_{HS} indicating better mutant-fitness in the HS-Screen than the
927 Growth-screen). Mutants exhibiting (1) poor growth in the HS-Screen (i.e., low FC-HS of
928 < 0.5 based on performance of *known HS-Sensitive *pB*-mutant-clones), and (2)

929 comparatively much better growth in the Growth-Screen (i.e., low PFS_{HS} of < 0.25) were
930 classified as HS-Sensitive in pooled phenotypic screens (indicated in red in Fig. 1E-F).
931 Mutants exhibiting poor fitness in both the Growth- and HS-Screens (FC-HS < 0.5 and
932 PFS_{HS} > 0.25) are indicated in Fig. 1E-F in yellow (n = 14). These double-sensitive
933 mutants were not included in our "HS-Sensitive" classification to avoid overinterpretation
934 of possibly-confounding phenotypes. We classified mutants displaying a slight growth
935 advantage in response to heat shock (FC-HS > 1.5, n = 28, indicated in the green box,
936 Fig.1E-F) as "HS-Tolerant". Mutants exhibiting neither sensitivity nor tolerance to heat
937 shock were classified as HS-Neutral (n = 49).
938
939 *Assigning drug- and oxidative stress-screen phenotypes*
940 Mutant fold-change in response to the given condition was calculated against an ideal-
941 growth control as above. Mutants in the top 25% of reads recovered in QIseq in the
942 screened condition were classified as Tolerant, while mutants in the bottom 25% were
943 classified as Sensitive.
944
945 *Comparative RNAseq between wild-type NF54 and two HS-Sensitive mutant parasite*
946 *lines in response to heat shock*
947 RNAseq experimental design is outlined in Fig. S11A. Briefly, highly synchronized ring-
948 stage cultures of wildtype NF54 and HS-Sensitive mutants *LRR5* and *DHC* were split
949 equally into four T75 flasks each. All parasites were grown at the normal human body
950 temperature (37C) to early ring-stage. Two flasks of each parasite-line were then
951 exposed to febrile temperatures (41C) for 8 hours, while the remaining two flasks were
952 allowed to continue to grow at 37C for 8 hours without exposure to heat-stress. This
953 temperature-cycling was repeated three times, just as we allowed for the pooled HS-
954 Screen. After the third round of heat-shock (Time 1, T^1), RNA was harvested

simultaneously from both conditions for RNAseq as in [19]. Parasite fold-change in response to HS was calculated at the time of sample-collection and verified mutant defects in response to HS as compared to NF54 (Fig S8B). RNA-seq was performed in-house on an Illumina MiSeq using a 300-cycle V2 MiSeq reagent kit.

RNA-seq data-analysis

RNA-seq reads from each sample were aligned to the *P. falciparum* reference genome (PlasmoDB version 28, RRID:SCR_013331). A maximum of one mismatch per read was allowed. The mapped reads from TopHat [51] were used to assemble known transcripts from the reference and their abundances were estimated using Cufflinks [52]. The expression level of each gene was normalized as FPKM (fragments per kilobase of exon per million mapped reads). We defined expressed genes as those having FPKM > 20 for at least one biological replicate at either 37°C or 41°C. The fold change of normalized gene expression between 41°C and 37°C was calculated for every biological replicate. Fold-change for genes not expressed in both temperatures was set equal to one. We conservatively filtered out genes in the top and bottom 10% of fold-change to remove outliers. We then fit a Gaussian model to the log2 fold change (*log2FC*) for every biological replicate using maximum log likelihood estimation to assess the fold-change distribution The p-value is calculated as the probability of estimated gaussian distribution higher than the observed *log2FC* (when observed *log2FC* $>$ the expection of estimated gaussian distribution), or lower than the observed *log2FC* (when observed *log2FC* $\leq$ the expection of estimated gaussian distribution). The false discovery rate (FDR) was calculated for each replicate. We defined genes for which FDR < 0.1 in both biological replicates as having significant fold-change in response to HS. Genes were assigned HS phenotype-categories based on significance and direction of HS-response. We assigned HS phenotype-categories for 2567 genes using these criteria (Table S3). Heat-shock

phenotypes as identified via pooled phenotypic screening and comparative RNAseq were highly correlated (Fig. S12A-B), supporting our methodology.

GO-term enrichment analyses

All GO-enrichment analyses were performed testing GO-terms mapped to genes in the category of interest against a background of GO-terms mapped to all other genes in the analysis. The GO-term database was created from the latest curated *P. falciparum* ontology available at the time of analysis, downloaded from GeneDB (accessed May 2, 2019) [53]. For enrichment-analysis in the 1K-library screens: Mutants were divided into HS-phenotype categories, and each category was tested for enrichment against a background of GO-terms mapped to the genes represented by the remainder of the 922 mutants in the screen using the weighted Fisher/elim hybrid-method of the TopGO package (v 1.0) available from Bioconductor [54] (Fig. 2B). For enrichment-analysis in comparative RNAseq data: a database of all GO-terms mapped to the 1298 genes which could be assigned a HS-phenotype in all three parasites was assembled. Genes were divided into HS phenotype-categories based on direction of fold-change (Up, Down, Unchanged) in response to HS in all three parasites, then evaluated for GO-term enrichment against the background GO-term database of all other genes in the analysis using the weighted-Fisher/elim hybrid-method of the TopGO package (Fig 3B, Table S3B-D). For enrichment of apicoplast-targeted genes by RNAseq HS-phenotype category: enrichment for each investigated GO-term *g* (The x-axis in Fig 4c, the ratio of up to down regulated genes) was calculated as the ratio (C_r) of up- vs. down-regulated genes mapped to GO-term *g* among all differential expressed apicoplast genes. This ratio (C) was also calculated for the genes mapped to GO-term *g* in the whole genome (the background distribution). The GO annotation for each gene was downloaded from GeneDB (accessed May 2, 2019). The fraction of HS-regulated apicoplast-genes to

non-HS-regulated apicoplast genes (C_n/C) was assessed for significance using the Fisher exact test (Fig 4C; Table S4A-B).

SUPPLEMENTARY FIGURE and TABLE LEGENDS

Figure S1. Schematic overview of the phenotypic screening pipeline. *pB*-mutant library resources from small (individual, well-characterized mutant-clones) to large (the 1K-Library, comprised of pools randomly selected from the Saturation-Library) were used to design carefully validated pooled screens at increasingly large scale. 1) to test the protocols using individual *pB*-mutant clones; 2) to develop pooled phenotypic screen method using pilot-library screen; 3) then we scale-up phenotypic screen using 1K-library; 4) parallel phenotype screens using pilot-library; 5) Transcriptional profiling via RNAseq compare the parasite response to heat shock between the wildtype and HS-sensitive mutants. High correlation between mutant-phenotypes in HS-screens and ART-screens indicated mechanistic overlap in response to both stressors. Iterative rounds of pooled-screening for various phenotypes over time enables higher-throughput functional-annotation of the *P. falciparum* genome.

Figure S2. Extended screening data against the pilot-library and summary.
A. Full drug-screening data for artemisinin-compounds AS and DHA, and proteasome-inhibitor Bortezomib (BTZ) against the pilot-library. HS-Sensitive mutants are significantly more sensitive to each drug than HS-Tolerant mutants. There is no significant relationship between *pB*-mutant sensitivity to any drug and mutant sensitivity in standard growth-conditions.
B. HS-Sensitive (red) and HS-Tolerant (green) mutants and their phenotypes across all pooled phenotypic screens. Mutants are clustered by HS-phenotype.

Figure S3. Mutants in members of the DV proteome, targets of ART alkylation, and putative interacting partners of K13 tend to be sensitive to HS.

A. 1k HS-Screen mutants are ordered by FC-HS from HS-Sensitive to HS-Tolerant. Mutants in digestive vacuole-associated proteins as defined by [26] are indicated in lavender dots. Gene-symbols for mutants with HS-sensitivity are labeled with black text (10 of 18 genes). Gene-symbols for HS-Neutral and HS-Tolerant mutants are labeled with grey text.

B. All mutants in ART alkylation-targets as defined by [9] included in the 1K HS-Screen.

C. HS-screen phenotypes of mutants in putative K13-interacting proteins as defined by [25].

Figure S4. A. Core proteasome-components are slightly but universally upregulated in response to HS as compared to other aggregately upregulated processes which have more heterogenous expression. Fold-change for most individual proteasome-components did not meet our threshold to be designated “upregulated”. ** Wilcoxon p-value < 1e-5.

B. Activation of pathways underlying DHA-mediated killing and febrile-temperature survival is directly inverse. Top. Model of DHA-mediated killing in *P. falciparum* adapted from [8]. Artemisinin (ART) damages and unfolds proteins, prevents folding of newly synthesized proteins, and inhibits the proteasome while at the same time activating E1/E2/E3 ubiquitin-machinery. Accumulation of toxic polyubiquitinated protein-substrates (S) overwhelms the cell and leads to death. **Bottom**. Model of parasite fever-response. Heat-stress causes globally damaged protein. The parasite increases the UPR as it inhibits E2/E3 ubiquitination to prevent accumulation of toxic, polyubiquitinated (Ub) protein-aggregates, while at the same time increasing its

capacity for proteasome-mediated degradation—ultimately enabling the parasite to resolve heat-shock-instigated stress and survive febrile-temperatures.

Figure S5. QIseq data-correlations within and between Pilot-Library Screens.

A. Pearson correlations between 5' and 3' QIseq data for 37°C_ideal-growth screen and 41°C_heat-shock screen indicate highly reproducible analyses across technical and biological replicates in both screens (Figure 1B).

B. Correlations within and between 37°C_ideal growth screen and 41°C_heat-shock screen QIseq data. The samples were collected in HS-Screens of the pilot-library include two bio-reps and three technical-reps (Figure 1A; Method, HS-Screen). High correlations of two bio-reps within both HS-screens and Growth-screens (HS-Screen, R=0.94; Growth-Screen, R=0.89) indicate the pilot-library screens are highly reproducible, and weak correlation between HS-screens and Growth-screens (R = ~0.42) suggests heat-shock exposure-conditions were sufficient to allow reproducible detection of mutants with specific selection response-phenotypes from pooled screening.

Figure S6. *pB*-mutant insertions are randomly distributed in the pilot-library and the 1K-library.

S6A. Comparative analysis of the *piggyBac* mutants' distribution patterns in coding vs noncoding regions between the pilot-library and 1K-library. Distribution patterns between intergenic regions and CDS are almost equal, with composition also reflecting the distribution of the saturation mutagenesis-library as a whole[6].

S6B. *pB*-mutants' distribution patterns across HS phenotype-categories of the 1K library. HS-Tolerant mutants were more likely associated with dispensable genes (genes with exonic insertions) than HS-Sensitive genes.

S6C. Distances between insertions of the 1K library are random. There is no significant difference in distance between each pair of neighboring *piggyBac* insertions of the 1K library and coordinates chosen by random sampling (p-value = 0.787, Mann-Whitney U test). Sampling was repeated 100x with sites randomly selected across all chromosomes.

Figure S7. Reproducibility of the 1K-library HS-Screen.

A. The 1K-library consists of randomly selected, uncloned large mixed-population pools (LMPP) of ~100 unique mutants per pool. Fifteen insertion-sites are duplicated in mutants of at least one other pool. Each of the 12 LMPP comprising the 1K-library (LMPP_1-6; LMPP_10-15) are indicated on the x-axis with violin plots showing the distribution of mutant fold change in response to heat shock (FC-HS) within that pool. FC-HS of the fifteen insertion-sites duplicated in at least one other pool are plotted in color, with insertion location-category indicated by shape.

B. FC-HS of duplicated insertional mutants are highly correlated across pools (Pearson correlation = 0.806), indicating high reproducibility of mutant phenotypes independent of mutant pool-composition. Insertions are represented as in plot A.

Figure S8. Reproducibility within and between the pilot-library and 1K-library HS-Screens.

A. Within- and between-library consistency indicates the robusticity of HS phenotype-assignments in pooled screening. Dynein heavy chain (DHC) gene-family mutants (two in DHA_12, PF3D7_1202300; one mutant of DHA_10, PF3D7_1023100) were consistently identified as HS-Sensitive in the pilot-library and across multiple pools of the 1K-library, as were representatives of FIKK-family genes.

B. Heatshock phenotypes are reproducible between the pilot library and the 1K-library. FC-HS of insertional mutants in genes represented in both the pilot library and the 1K-library (n = 16 genes; colored points) are highly correlated (Pearson correlation = 0.702). Insertion coordinate in the pilot library is indicated on the left of the '||', while insertion coordinate of the mutant in the same gene in the 1K-library is to the right. Distance between the pilot-library insertion and the 1K-library insertion is indicated by shape (maximum distance = 1kb).

Figure S9. Phenotypic Fitness-Score in HS (PFS_{HS}) distribution across mutant HS phenotype-classifications in the 1K-Library screen. See Table S2 and Methods for PFS_{HS} calculation details. HS-Sensitive mutants (mutants displaying defective growth in response to heat shock but not in response to ideal growth conditions) are assigned the lowest PFS_{HS}, while HS-Tolerant mutations are assigned the highest PFS_{HS}.

Figure S10. Qlseq data-correlations within and between Pilot-Library phenotypic screens: drugs and oxidative stress.
All pooled phenotypic screens of pilot-library (AS, DHA, BTZ, oxidative stress, ideal growth) were performed in biological duplicate, high correlations of bio-reps indicate highly reproducible analyses across all pilot-library phenotype screens.

Figure S11. Methods and validation for comparative RNAseq.
A. RNA sample-collection methods for wildtype malaria-parasite NF54 vs. two HS-Sensitive *pB*-mutant clones **Δ*DHC* (PB4) and Δ*LRR5* (PB31)** in response to febrile temperatures. Assays were performed in biological duplicate.

B. Validation of HS-Sensitive mutant-clones during RNA-Seq Sample preparation**.** Both mutants grown individually had growth-defects in response to HS as compared to NF54.

Figure S12. Complementary methods (pooled phenotypic screening, phenotypic transcriptional profiling of HS-Sensitive mutants vs. wildtype in response to heat stress) indicate genes driving the parasite heat-stress response.

A. HS-Sensitive *pB* mutants tend to have mutations in genes that have significant changes in expression in response to heat-stress, while mutants that are neutral to or tolerant of heat-stress tend to have mutations in genes that are not regulated in response to heat-stress.

B. *pB* mutants in genes normally up-regulated in response to heat-stress grow poorly in response to heat-stress (i.e., have significantly lower phenotypic fitness-scores) than mutants in genes that are neutral or down-regulated in response to heat-stress.

Supplemental Tables:

Table S1A. Pooled HS-Screen results of the *P. falciparum pB*-mutant pilot-library (n = 128, Fig. 1).

S1B. Summary counts of pilot-library mutants by phenotype-category in pooled screening.

S1C. GeneIDs, functional information, and distance to the insertion-site for neighboring genes on both sides of *piggyBac* insertions of the pilot library.

Table S2A. Pooled HS-Screen results of the 1K-Library (n = 922, Fig. 2).

S2B. Summary counts of 1K-library mutants by phenotype-category in pooled screening.

S2C. GeneIDs, functional information, and distance to the insertion-site for neighboring genes on both sides of *piggyBac* insertions of the 1K-library.

Table S3. Comparative RNAseq-results between NF54 and HS-Sensitive mutant-clones *ΔLRR5* and *ΔDHC* in response to heat-shock (Fig. 3).

S3A. All genes classified into HS response-categories in NF54 with or without exposure to heat-shock using RNAseq data (n = 2567). HS-classifications for each gene in two HS-Sensitive mutant-lines are indicated where available. Criteria for inclusion: NF54 expression above threshold (FPKM > or = 20 for at least one replicate in at least one temperature-condition) and FC-HS supported by two biological replicates.

S3B. Genes included in functional enrichment-analyses. Criteria for inclusion: all genes with expression above threshold AND agreement between replicates as to HS fold-change classification for all three parasite lines (n = 1298).

S3C. Enriched GO-terms for specified HS-response-categories as included in Figure 3B. “Annotated”: the number of genes annotated to a given GO-term included in the analysis for all HS response-categories. “Significant”: the number of genes annotated to a given GO-term in the HS response-category being tested for enrichment.

S3D. Full functional enrichment-results for all HS response-categories.

Table S4. Apicoplast genes regulated in response to HS (Fig. 4).

S4A. Apicoplast-targeted genes regulated in response to HS (RNAseq data used in Figure 4A-B).

S4B. GO-terms mapped to HS-regulated apicoplast-targeted genes (pertains to Fig. 4C).

S4C. Pooled heatshock-screen data for all mutants associated with processes of interest highlighted in Figures 4D-E.

S4D. Comparative wildtype/HS-Sensitive mutant RNAseq data for genes associated with processes of interest highlighted in Figure 4E.

Table S5. Drug- and oxidative stress-screen results of the pilot library (n = 128).

Table S6A-B. Data pertaining to Figure 5C and 5D.

Table S7. QIseq dataset accession numbers.

References

1. WHO. World Malaria Report. *World Health Organization*, (2018).

2. Gardner MJ*, et al.* Genome sequence of the human malaria parasite *Plasmodium falciparum*. *Nature* **419**, 498-511 (2002).

3. Aurrecoechea C*, et al.* PlasmoDB: a functional genomic database for malaria parasites. *Nucleic Acids Res* **37**, D539-543 (2009).

4. Oakley MS, Gerald N, McCutchan TF, Aravind L, Kumar S. Clinical and molecular aspects of malaria fever. *Trends in parasitology* **27**, 442-449 (2011).

5. Oakley MSM*, et al.* Molecular factors and biochemical pathways induced by febrile temperature in intraerythrocytic *Plasmodium falciparum* parasites. *Infection and immunity* **75**, 2012-2025 (2007).

6. Zhang M*, et al.* Uncovering the essential genes of the human malaria parasite *Plasmodium falciparum* by saturation mutagenesis. *Science* **360**, (2018).

7. Rocamora F*, et al.* Oxidative stress and protein damage responses mediate artemisinin resistance in malaria parasites. *PLoS Pathog* **14**, e1006930-e1006930 (2018).

8. Bridgford JL*, et al.* Artemisinin kills malaria parasites by damaging proteins and inhibiting the proteasome. *Nature Communications* **9**, 3801 (2018).

9. Ismail HM*, et al.* Artemisinin activity-based probes identify multiple molecular targets within the asexual stage of the malaria parasites *Plasmodium falciparum* 3D7. *Proceedings of the National Academy of Sciences* **113**, 2080-2085 (2016).

10. Mok S*, et al.* Drug resistance. Population transcriptomics of human malaria parasites reveals the mechanism of artemisinin resistance. *Science* **347**, 431-435 (2015).

11. Yang T*, et al.* Decreased K13 Abundance Reduces Hemoglobin Catabolism and Proteotoxic Stress, Underpinning Artemisinin Resistance. *Cell Reports* **29**, 2917-2928.e2915 (2019).

12. Birnbaum J*, et al.* A Kelch13-defined endocytosis pathway mediates artemisinin resistance in malaria parasites. *Science* **367**, 51 (2020).

13. Bronner IFF*, et al.* Quantitative Insertion-site Sequencing (QIseq) for high throughput phenotyping of transposon mutants. *Genome Research*, (2016).

14. Balu B*, et al. piggyBac* is an effective tool for functional analysis of the *Plasmodium falciparum* genome. *BMC microbiology* **9**, 83 (2009).

15. Thomas P*, et al.* Phenotypic Screens Identify Parasite Genetic Factors Associated with Malarial Fever Response in *Plasmodium falciparum piggyBac* Mutants. *mSphere* **1**, (2016).

16. Bushell E*, et al.* Functional Profiling of a *Plasmodium* Genome Reveals an Abundance of Essential Genes. *Cell* **170**, 260-272.e268 (2017).

17. Gisselberg JE, Zhang L, Elias JE, Yeh E. The Prenylated Proteome of *Plasmodium falciparum* Reveals Pathogen-specific Prenylation Activity and Drug Mechanism-of-action. *Molecular & Cellular Proteomics* **16**, S54-S64 (2017).

18. Suazo KF, Schaber C, Palsuledesai CC, Odom John AR, Distefano MD. Global proteomic analysis of prenylated proteins in *Plasmodium falciparum* using an alkyne-modified isoprenoid analogue. *Scientific Reports* **6**, 38615 (2016).

19. Gibbons J*, et al.* Altered expression of K13 disrupts DNA replication and repair in *Plasmodium falciparum*. *BMC Genomics* **19**, 849 (2018).

20. Krishnan KM, Williamson KC. The proteasome as a target to combat malaria: hits and misses. *Translational Research* **198**, 40-47 (2018).

21. Ng CL, Fidock DA, Bogyo M. Protein Degradation Systems as Antimalarial Therapeutic Targets. *Trends in Parasitology* **33**, 731-743 (2017).

22. Ariey F*, et al.* A molecular marker of artemisinin-resistant *Plasmodium falciparum* malaria. *Nature* **505**, 50-55 (2014).

23. Tilley L, Straimer J, Gnädig NF, Ralph SA, Fidock DA. Artemisinin Action and Resistance in *Plasmodium falciparum*. *Trends in parasitology* **32**, 682-696 (2016).

24. Bhattacharjee S*, et al.* Remodeling of the malaria parasite and host human red cell by vesicle amplification that induces artemisinin resistance. *Blood* **131**, 1234-1247 (2018).

25. Gnädig NF*, et al.* Insights into the intracellular localization, protein associations and artemisinin resistance properties of *Plasmodium falciparum* K13. *PLoS Pathog* **16**, e1008482 (2020).

26. Lamarque M*, et al.* Food vacuole proteome of the malarial parasite *Plasmodium falciparum*. *Proteomics Clin Appl* **2**, 1361-1374 (2008).

27. Dogovski C*, et al.* Targeting the Cell Stress Response of *Plasmodium falciparum* to Overcome Artemisinin Resistance. *PLOS Biology* **13**, e1002132 (2015).

28. White JK, Handa S, Vankayala SL, Merkler DJ, Woodcock HL. Thiamin Diphosphate Activation in 1-Deoxy-d-xylulose 5-Phosphate Synthase: Insights into the Mechanism and Underlying Intermolecular Interactions. *J Phys Chem B* **120**, 9922-9934 (2016).

29. Imlay L, Odom AR. Isoprenoid Metabolism in Apicomplexan Parasites. *Current Clinical Microbiology Reports* **1**, 37-50 (2014).

30. Kennedy K*, et al.* Delayed death in the malaria parasite *Plasmodium falciparum* is caused by disruption of prenylation-dependent intracellular trafficking. *PLOS Biology* **17**, e3000376 (2019).

31. Howe R, Kelly M, Jimah J, Hodge D, Odom AR. Isoprenoid biosynthesis inhibition disrupts Rab5 localization and food vacuolar integrity in *Plasmodium falciparum*. *Eukaryot Cell* **12**, 215-223 (2013).

32. Pandey AV, Tekwani BL, Singh RL, Chauhan VS. Artemisinin, an endoperoxide antimalarial, disrupts the hemoglobin catabolism and heme detoxification systems in malarial parasite. *J Biol Chem* **274**, 19383-19388 (1999).

33. del Pilar Crespo M*, et al.* Artemisinin and a series of novel endoperoxide antimalarials exert early effects on digestive vacuole morphology. *Antimicrob Agents Chemother* **52**, 98-109 (2008).

34. Sussmann RAC, Fotoran WL, Kimura EA, Katzin AM. *Plasmodium falciparum* uses vitamin E to avoid oxidative stress. *Parasit Vectors* **10**, 461-461 (2017).

35. Mène-Saffrané L. Vitamin E Biosynthesis and Its Regulation in Plants. *Antioxidants (Basel)* **7**, 2 (2017).

36. Estévez JM, Cantero A, Reindl A, Reichler S, León P. 1-Deoxy-d-xylulose-5-phosphate Synthase, a Limiting Enzyme for Plastidic Isoprenoid Biosynthesis in Plants. *Journal of Biological Chemistry* **276**, 22901-22909 (2001).

37. Zhang F*, et al.* Molecular Characterization of the 1-Deoxy-D-Xylulose 5-Phosphate Synthase Gene Family in Artemisia annua. *Frontiers in Plant Science* **9**, (2018).

38. Heuston S, Begley M, Gahan CGM, Hill C. Isoprenoid biosynthesis in bacterial pathogens. *Microbiology* **158**, 1389-1401 (2012).

39. Brunetti C, Guidi L, Sebastiani F, Tattini M. Isoprenoids and phenylpropanoids are key components of the antioxidant defense system of plants facing severe excess light stress. *Environmental and Experimental Botany* **119**, 54-62 (2015).

40. Mathews ES, Jezewski AJ, Odom John AR. Protein prenylation and Hsp40 in thermotolerance of *Plasmodium falciparum* malaria parasites. *bioRxiv*, 842468 (2019).

41. Clarke A. The thermal limits to life on Earth. *International Journal of Astrobiology* **13**, 141-154 (2014).

42. Kobayashi Y*, et al.* Algae sense exact temperatures: small heat shock proteins are expressed at the survival threshold temperature in *Cyanidioschyzon merolae* and *Chlamydomonas reinhardtii*. *Genome biology and evolution* **6**, 2731-2740 (2014).

43. Li GQ, Arnold K, Guo XB, Jian HX, Fu LC. Randomised comparative study of mefloquine, qinghaosu, and pyrimethamine-sulfadoxine in patients with falciparum malaria. *Lancet* **2**, 1360-1361 (1984).

44. Kirkman LA*, et al.* Antimalarial proteasome inhibitor reveals collateral sensitivity from intersubunit interactions and fitness cost of resistance. *Proceedings of the National Academy of Sciences* **115**, E6863 (2018).

45. Oberstaller J, Otto TD, Rayner JC, Adams JH. Essential Genes of the Parasitic Apicomplexa. *Trends Parasitol*, (2021).

46. Oberstaller J, Zhang M, Wang C. RNAseq dataset: Malaria-parasite survival of host fever is linked to artemisinin resistance) (2020).

47. Boucher MJ, Yeh E. Disruption of Apicoplast Biogenesis by Chemical Stabilization of an Imported Protein Evades the Delayed-Death Phenotype in Malaria Parasites. *mSphere* **4**, e00710-00718 (2019).

48. Ralph SA*, et al.* Metabolic maps and functions of the *Plasmodium falciparum* apicoplast. *Nature Reviews Microbiology* **2**, 203 (2004).

49. Guggisberg AM*, et al.* A sugar phosphatase regulates the methylerythritol phosphate (MEP) pathway in malaria parasites. *Nature Communications* **5**, 4467 (2014).

50. Cyrklaff M*, et al.* Oxidative insult can induce malaria-protective trait of sickle and fetal erythrocytes. *Nature Communications* **7**, 13401 (2016).

51. Trapnell C, Pachter L, Salzberg SL. TopHat: discovering splice junctions with RNA-Seq. *Bioinformatics* **25**, 1105-1111 (2009).

52. Trapnell C*, et al.* Transcript assembly and quantification by RNA-Seq reveals unannotated transcripts and isoform switching during cell differentiation. *Nat Biotech* **28**, 511-515 (2010).

53. Logan-Klumpler FJ*, et al.* GeneDB--an annotation database for pathogens. *Nucleic acids research* **40**, D98-108 (2012).

54. Alexa A, Rahnenfuhrer J, Lengauer T. Improved scoring of functional groups from gene expression data by decorrelating GO graph structure. *Bioinformatics* **22**, 1600-1607 (2006).

Figure 1. Pooled screens of an extensively characterized *pB*-mutant pilot-clone-library allow robust identification of heat-shock phenotypes

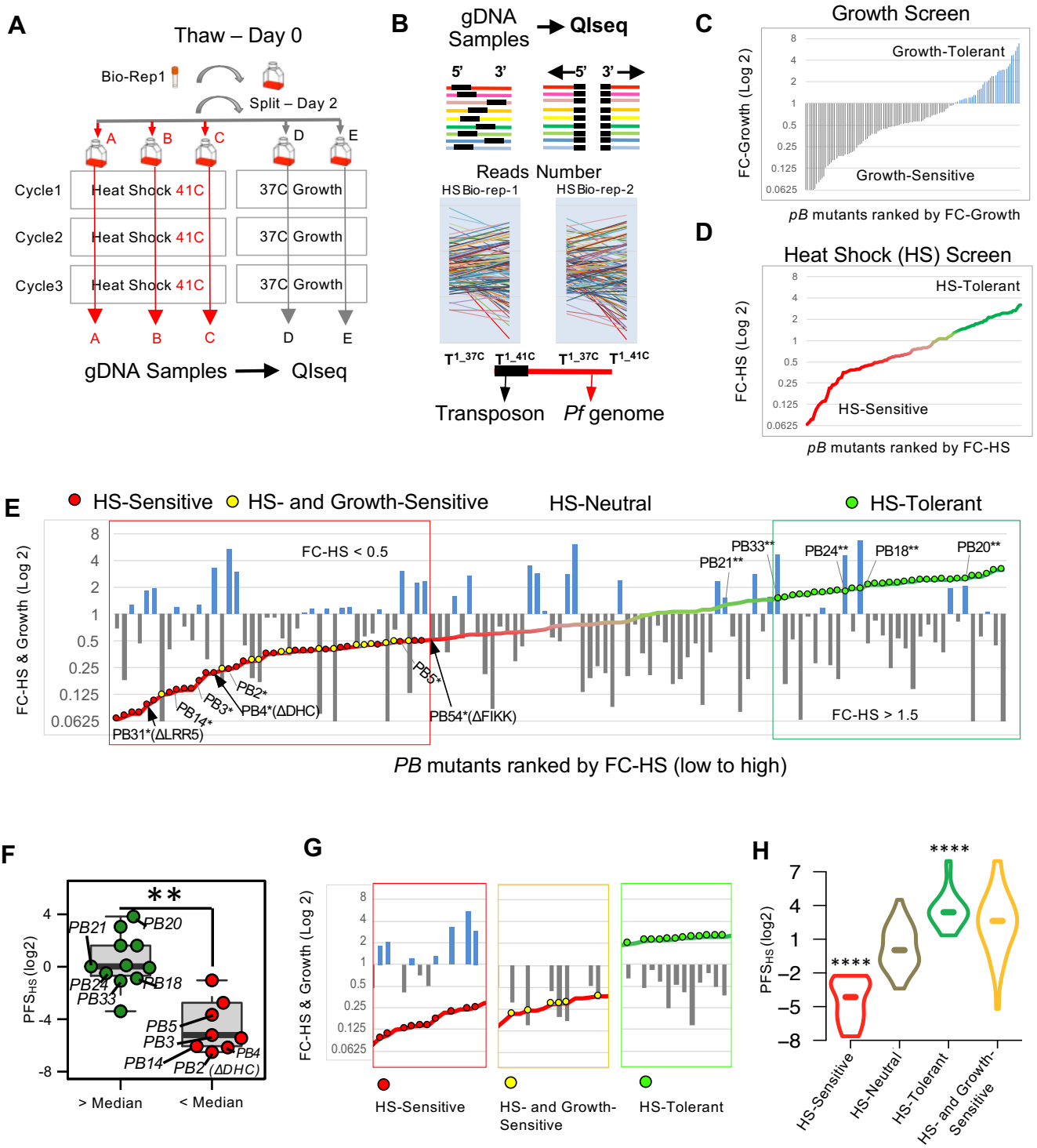

Figure 2. Pooled phenotypic screens scaled up to a 1K-*pB*-mutant library enable identification of processes driving the *P. falciparum* heat-shock response

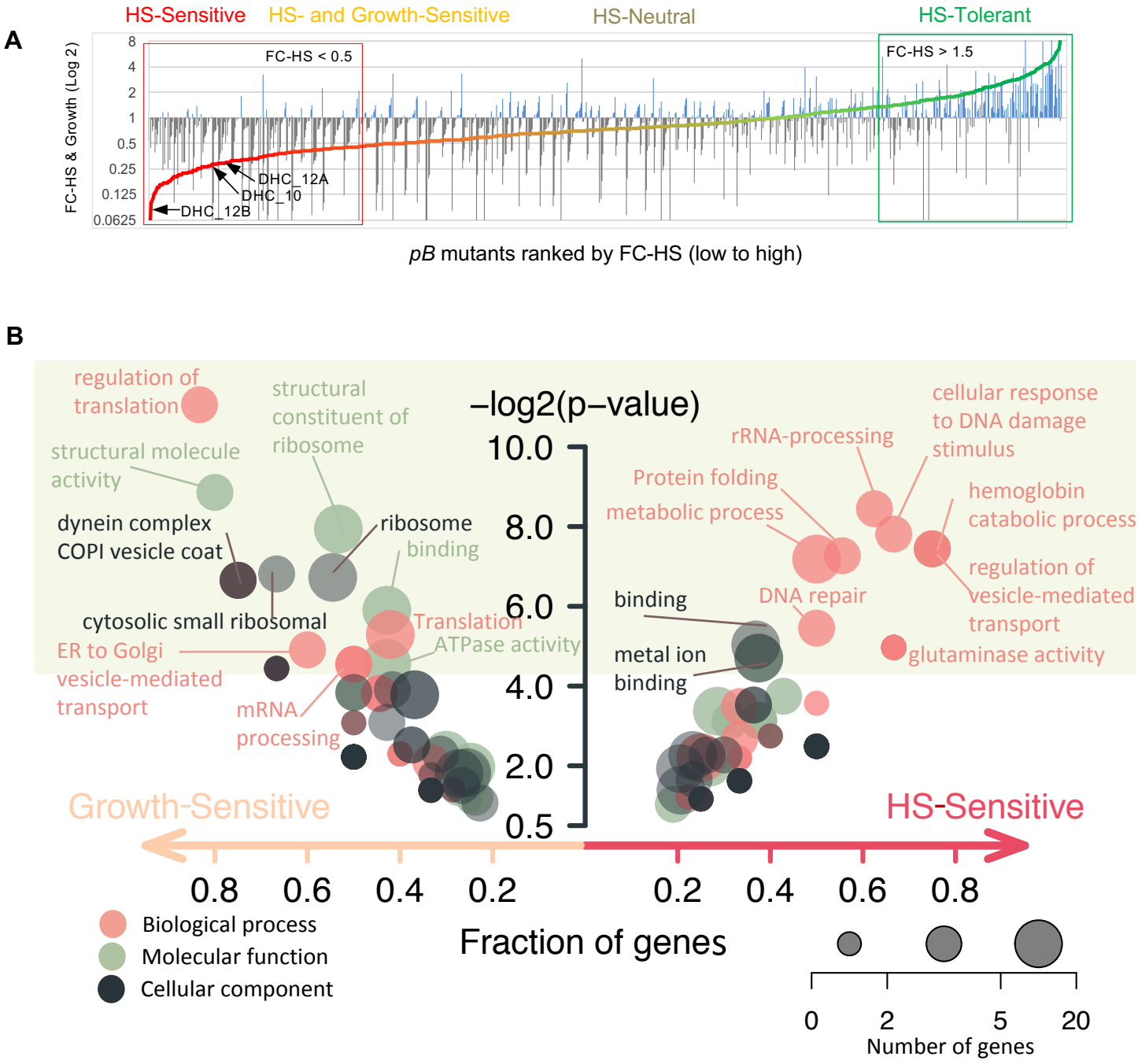

Figure 3.

Unfolded protein response, apicoplast-targeted and mitochondria-targeted stress-response pathways are critically dysregulated in functionally unrelated HS-Sensitive mutant clones.

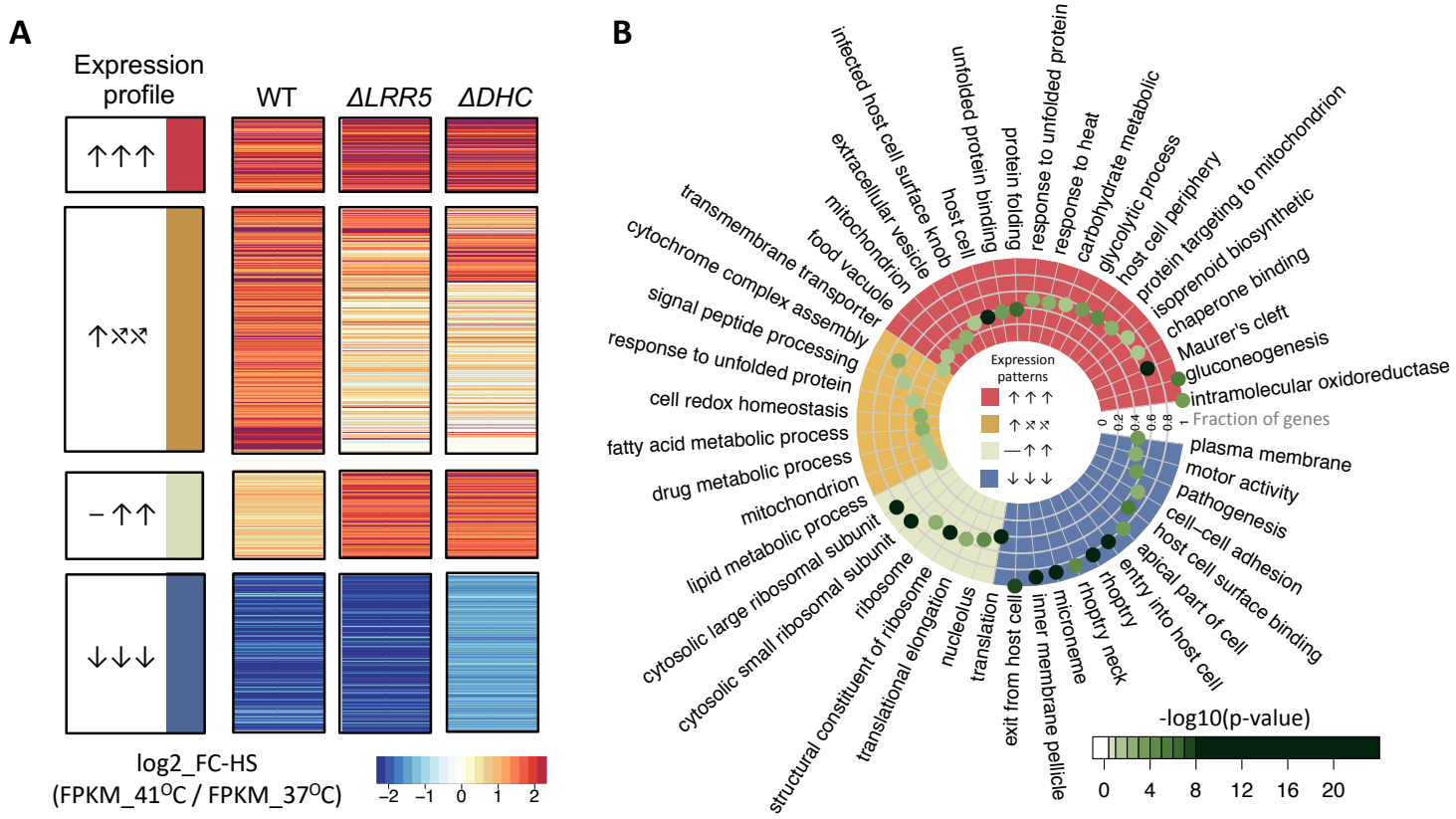

C

Expression profile (HS)	Gene ID	Symbol	Gene Description
↑↑↑	PF3D7_0708400	HSP90	heat shock protein 90
	PF3D7_0209300	IspF	2C-methyl-D-erythritol 2,4-cyclodiphosphate synthase
	PF3D7_1119100*	tRNA-m1G*	tRNA m(1)G methyltransferase, putative
	PF3D7_1037100	PyKII	pyruvate kinase 2
	PF3D7_1439900	TIM	triosephosphate isomerase
	PF3D7_1115700	FP2A	cysteine proteinase falcipain 2a
	PF3D7_0810800	PPPK-DHPS	hydroxymethyldihydropterin pyrophosphokinase…
	PF3D7_1342800	PEPCK	phosphoenolpyruvate carboxykinase
	PF3D7_1129400	NOP2	rRNA (cytosine-C(5))-methyltransferase, putative
	PF3D7_1442500	N/A	geranylgeranyl transferase type-2 subunit …
	PF3D7_0602500	N/A	geranylgeranyltransferase, putative
↑⇗⇗	PF3D7_1337200*	DXS*	1-deoxy-D-xylulose 5-phosphate synthase
	PF3D7_0218300*	N/A	apicoplast RNA methyltransferase (apico-RNA-methyl)
	PF3D7_1239600	ThzK	hydroxyethylthiazole kinase
	PF3D7_1214200	SET5	histone-lysine N-methyltransferase, putative
	PF3D7_1128400	FPPS/GGPPS	geranylgeranyl pyrophosphate synthase, putative
	PF3D7_1437400	PANK2	pantothenate kinase, putative
	PF3D7_1426200	PRMT1	protein arginine N-methyltransferase 1
	PF3D7_1103400	SufD	FeS cluster assembly protein SufD
	PF3D7_0628800	GATB	glutamyl-tRNA(Gln) amidotransferase subunit B
	PF3D7_1443900	HSP90	heat shock protein 90, putative
	PF3D7_1019800	N/A	tRNA methyltransferase, putative
	PF3D7_1450900	N/A	acetyl-CoA acetyltransferase, putative
	PF3D7_0218600	N/A	conserved Plasmodium protein, unknown function

Figure 4. Apicoplast isoprenoid biosynthesis is critical for *P. falciparum* survival of febrile temperatures

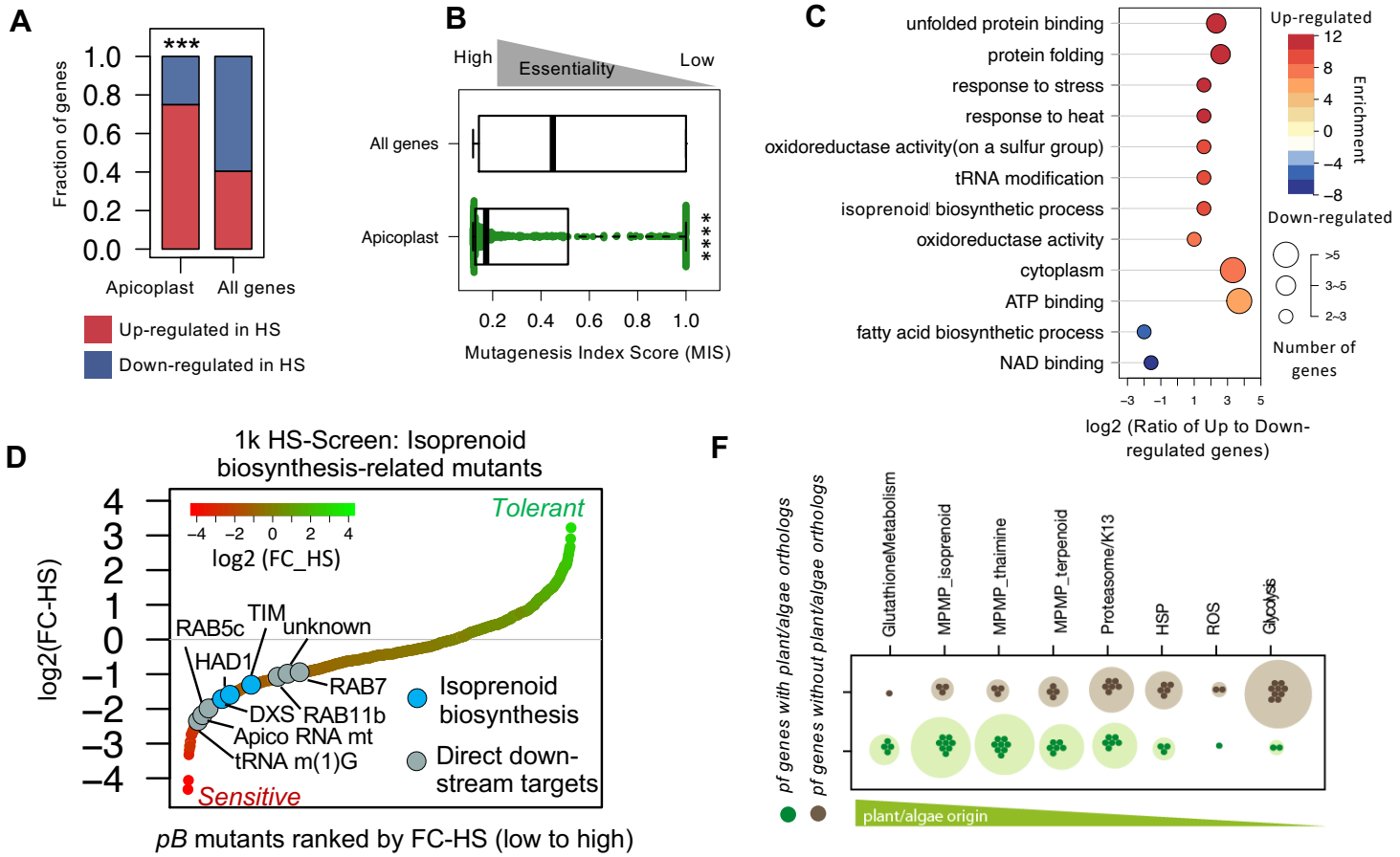

Figure 5. Increased sensitivity to fever is directly correlated with increased sensitivity to artemisinin in the malaria parasite